# AN APPROACH FOR THE AUTOMATIC SEGMENTATION OF HIGH RESOLUTION SATELLITE IMAGES INTO AGRICULTURAL FIELDS

# YÜKSEK ÇÖZÜNÜRLÜKLÜ UYDU GÖRÜNTÜLERİNİN TARIMSAL PARSELLERE OTOMATİK SEGMENTASYONU İÇİN BİR YAKLAŞIM

**ALIREZA RAHIMZADEGANASL**

**PROF. DR. MUSTAFA TÜRKER**

**Supervisor**

Submitted to Institute of Sciences of Hacettepe University
as a Partial Fulfillment to the Requirements
for the Award of the Degree of Master of Science
in Geomatics Engineering

August 2015

This work named **"AN APPROACH FOR THE AUTOMATIC SEGMENTATION OF HIGH RESOLUTION SATELLITE IMAGES INTO AGRICULTURAL FIELDS"** by **ALIREZA RAHIMZADEGANASL** has been approved as a thesis for the Degree of **MASTER OF SCIENCE IN GEOMATICS ENGINEERING** by the below mentioned Examining Committee Members.

Prof. Dr. Mustafa TÜRKER
Head and Supervisor .....

Assoc. Prof. Dr. Cevdet Coşkun AYDIN
Member .....

Asst. Prof. Dr. Kamil TEKE
Member .....

Asst. Prof. Dr. Emre SÜMER
Member .....

Asst. Prof. Dr. Baran USLU
Member .....

This thesis has been approved as a thesis for the Degree of **MASTER OF SCIENCE IN GEOMATICS ENGINEERING** by Board of Directors of the institute for Graduate Studies in Science and Engineering.

Prof. Dr. Fatma SEVİN DÜZ
Director of the Institute of
Graduate School of Science and Engineering

*To My Parents*

*And My Lovely Deniz*

# ETHICS

In this thesis study, prepared in accordance with the spelling rules of Institute of Graduate Studies in Science and Engineering of Hacettepe University,

I declare that

- all the information and documents have been obtained in the base of the academic rules,
- all audio-visual and written information and results have been presented according to the rules of scientific ethics,
- in case of using other Works, related studies have been cited in accordance with the scientific standards,
- all cited studies have been fully referenced,
- I did not do any distortion in the data set,
- and any part of this thesis has not been presented as another thesis study at this or any other university.

10/08/2015

**ALIREZA RAHIMZADEGANASL**

# ABSTRACT

## AN APPROACH FOR THE AUTOMATIC SEGMENTATION OF HIGH RESOLUTION SATELLITE IMAGES INTO AGRICULTURAL FIELDS

**Alireza Rahimzadeganasl**
**Master of Sciences, Department of Geomatics Engineering**
**Supervisor: Prof. Dr. Mustafa TÜRKER**
**August 2015, 89 pages**

Monitoring and management of land use plays an important role in the economic development of agriculture regions in the world. Satellite images have become very popular data source for crop mapping in agricultural areas. With this respect, the extraction of agricultural land parcels is critical for crop classification and further field-based analysis operations. An efficient image analysis procedure is needed to automatically extract agricultural fields with the minimum user intervention. When performed on field-by-field basis, agricultural crop classification produces much better results. Field-based image classification techniques use approaches that assign crop labels for the agricultural fields individually. The classification is performed within permanent field boundaries which are stored in a geographic information system (GIS) database as vector dataset.

In this study, a field-based segmentation approach is proposed to extract sub-fields within permanent boundaries of agricultural fields from high resolution remotely sensed imagery. The sub-field extraction operation is carried out one field at a time by means of processing each field separately. The developed approach is based on the extension of the watershed algorithm for multispectral image segmentation. Watershed transformation is a powerful algorithm for image segmentation. First, a gradient magnitude image is calculated from the generated intensity image using

the Sobel edge detection operator. Next, the foreground markers, which will be used in watershed transformation, are extracted using Otsu's thresholding method. To automate the marker extraction procedure, Otsu's thresholding method is employed in an optimized iterative manner. The extracted foreground markers are used in the remainder of the process after performing some morphological operations. A marker controlled watershed segmentation is then carried out for the extraction of sub-fields that stay within permanent boundaries of agricultural fields.

The developed approach was tested in an agricultural area locate near the town of Karacabey, Bursa in North-West of Turkey. The high resolution satellite images used include the Spot5 multispectral (XS) image acquired in 22 July 2004, the Ikonos multispectral (XS) image acquired in 15 July 2004 and the QuickBird multispectral (XS) and pansharpened (PS) images acquired in 13 August 2004. The achieved results are quite promising. The overall accuracies of the sub-fields extracted through developed automatic approach were computed to be 80.34%, 89.72%, 83.24% and 78.88% for the Spot5 (XS), Ikonos (XS), QuickBird (XS) and QuickBird (PS) images, respectively.

**Keywords:** Agricultural, Image Segmentation, Field-Based, Gradient Image, Otsu's Thresholding, Marker Controlled Watershed.

# ÖZET

## YÜKSEK ÇÖZÜNÜRLÜKLÜ UYDU GÖRÜNTÜLERİNİN TARIMSAL PARSELLERE OTOMATİK OLARAK SEGMENTASYONU İÇİN BİR YAKLAŞIM

**Alireza Rahimzadeganasl**
**Yüksek Lisans, Geomatik Mühendisliği bölümü**
**Tez Danışmanı: Prof. Dr. Mustafa TÜRKER**
**Ağustos 2015, 89 sayfa**

Arazi kullanımı İzlemesi ve yönetimi, dünyadaki tarım bölgelerinin ekonomik gelişmesinde önemli bir rol oynar. Uydu görüntüleri tarım alanlarında ürün haritalaması için popüler veri kaynağıdır. Bu bağlamda, tarım parsellerinin çıkarımı, ürün sınıflandırması ve parsel-tabanlı analizler için, kritik öneme sahiptir. Tarımsal parselleri otomatik çıkarmak için kullanıcı ihtiyacı minimum olan etkili bir görüntü analizi yöntemi gereklidir. Tarımsal ürün sınıflandırması, parsel-parsel yapıldığı zaman çok daha iyi sonuçlar üretir. Parsel tabanlı görüntü sınıflandırma teknikleri, tarımsal parsellere ürün etiketini bireysel atayan yaklaşımlar kullanır. Sınıflandırma, bir coğrafi bilgi sistemi (CBS) veri tabanında vektör veri seti olarak depolanan sabit sınırlar içinde gerçekleştirilir.

Bu çalışmada, sabit tarımsal parseller içinde alt parselleri yüksek çözünürlüklü uydu görüntülerinden çıkarmak için bir parsel-tabanlı bölütleme yaklaşımı önerilmektedir. Alt parsel çıkarma işlemi her parsel ayrı işlenmek suretiyle, parsel-parsel gerçekleştirilir. Geliştirilen yaklaşım, çok bantlı görüntü bölütlemesi için havza algoritmasının genişletilmesine dayalıdır. Havza dönüşümü görüntü bölütlemesi için güçlü bir algoritmadır. İlk olarak, oluşturulan yoğunluk görüntüsünden, Sobel kenar bulma operatörü kullanılarak, gradyan büyüklüğü görüntüsü, hesaplanır. Sonra,

Otsu’nun eşikleme yöntemi kullanılarak, havza dönüşümünde kullanılacak ön işaretleyiciler çıkarılır. İşaretçileri çıkarma işlemini otomatik hale getirmek için, Otsu yöntemi optimize iteratif bir şekilde kullanılır. Çıkarılan ön işaretleyiciler, bazı morfolojik işlemler uygulandıktan sonra, geriye kalan işlem adımlarında kullanılır. Sonra, tarımsal parseller kalıcı sınırların içinde kalan alt alanların çıkarılması için işaretleyici kontrollü havza bölütlemesi gerçekleştirilir.

Geliştirilen yaklaşım, Türkiye'nin kuzey-batısında yer alan Bursa ili, Karacabey ilçesinde bir tarım alanı üzerinde test edilmiştir. Kullanılan yüksek çözünürlüklü uydu görüntüleri, 22 Temmuz 2004 tarihli çok bantlı Spot5 görüntüsü, 15 Temmuz 2004 tarihli çok bantlı Ikonos görüntüsü ve 13 Ağustos 2004 tarihli çok bantlı ve keskinleştirilmiş QuickBird görüntüleridir. Elde edilen sonuçlar oldukça umut vericidir. Geliştirilen otomatik yaklaşım ile çıkarılan alt alanların genel doğrulukları, çok bantlı Spot5, çok bantlı Ikonos, çok bantlı QuickBird ve keskinleştirilmiş QuickBird görüntüleri için sırasıyla % 80.34, % 89.72, % 83.24 ve % 78.88 olarak hesaplanmıştır.

**Anahtar Kelimeler:** Tarım, Görüntü Bölütleme, Alan Bazlı, Gradian Görüntüsü, Otsu’nun eşikleme yöntemi, işaretleyici kontrollü havza.

# ACKNOWLEDGMENTS

I would like to express my sincere gratitude to my advisor Prof. Dr. Mustafa TÜRKER for the continuous support of my MSc study and research, for his patience, motivation, enthusiasm, and immense knowledge.

I would also like to thank my parents, Mr. Rahimzadeganasl and Mrs. Miralilou for their continuous support and encouragement during my education and throughout my life and for giving me the opportunity of an education from the one of the best institutions. I would like to dedicate this work to them for all that they have done for me.

I would also like to thank my beautiful girlfriend, Ms. Gholizadeh who has been there for me and motivated me to do my studies and researches.

I also want to mention and thank my friends Mr. Farshi, Mr. Khalilzade and Mr. Fardhal for helping me throughout my thesis and also my friends who have made my stay in Ankara, enjoyable and memorable.

# TABLE OF CONTENTS

**Page**

ABSTRACT ..... i
ÖZET ..... iii
ACKNOWLEDGMENTS ..... v
TABLE OF CONTENTS ..... vi
LIST OF TABLES ..... viii
LIST OF FIGURES ..... ix
SYMBOLS AND ABBREVIATIONS ..... xi
1. INTRODUCTION ..... 1
1.1. The Thesis' Goals ..... 3
1.2. Contributions ..... 3
1.3. Thesis Outline ..... 4
1.4. Software ..... 4
2. LITERATURE REVIEW ..... 6
2.1. Image Segmentation ..... 6
2.2. The Watershed Algorithm ..... 11
2.3. Marker Controlled Watershed ..... 12
3. METHODOLOGY ..... 13
3.1. Preprocessing ..... 15
3.1.1. RGB to Intensity Transformation ..... 15
3.1.2. Smoothing Spatial Filters ..... 16
3.1.2.1. Average Filter ..... 16
3.1.2.2. Median Filter ..... 17
3.1.3. Image Gradient ..... 18
3.2. Inner Segmentation ..... 21
3.2.1. Image Thresholding ..... 21
3.2.1.1. Fundamentals of Image Thresholding ..... 21
3.2.1.2. Optimum Global Thresholding Using Otsu's Method ..... 22
3.2.2. First Step of Otsu Thresholding ..... 24
3.2.3. Second Step of Otsu Thresholding ..... 25
3.2.4. Morphological Processing ..... 26
3.2.4.1. Morphological Erosion ..... 27

3.2.4.2. Morphological Hole Filling ..... 28
3.2.4.3. Using Mathematical Morphology in the Proposed Method ..... 29
3.2.5. Reversing and Union Step..... 31
3.3. Watershed Segmentation ..... 33
3.3.1. Watershed Segmentation Using the Gradient ..... 33
3.3.2. Marker Controlled Watershed Segmentation..... 34
3.4. Accuracy Assessment ..... 36
4. RESULTS AND DISCUSSIONS ..... 39
4.1. Study Area..... 39
4.2. Data Sets..... 39
4.2.1. Satellite Imagery Data ..... 40
4.2.2. Field Boundary Data..... 41
4.3. The Results of Intensity Image ..... 41
4.3.1. The Results of Ikonos Multispectral (XS) Images ..... 45
4.3.2. The Results of QuickBird Multispectral (XS) Images ..... 50
4.3.3. The Results of QuickBird Pan Sharpened (PS) Images ..... 55
4.3.4. The Results of Spot5 Multispectral (XS) Images ..... 59
4.3.5. Comparison of All Four Images ..... 64
5. CONCLUSIONS AND RECOMMENDATIONS ..... 65
5.1. Conclusions..... 65
5.2. Recommendations ..... 66
REFERENCES..... 68
CURRICULUM VITAE..... 74

# LIST OF TABLES

**Page**

**Table 1.** Used raster data..... 40
**Table 2.** The spectral and spatial specifications of the satellite data used..... 40
**Table 3.** The sizes of the test fields..... 42
**Table 4.** The number of subfields in each field..... 42
**Table 5.** The number of subfields which were detected through the proposed segmented method..... 43
**Table 6.** The filter sizes used for each imagery system ..... 43
**Table 7.** The overall accuracies computed for each group of images ..... 44
**Table 8.** The grouping of results by the number of segments ..... 45
**Table 9.** The results of Ikonos XS images ..... 46
**Table 10.** For Ikonos XS imagery the grouping of the test fields based on their accuracy values..... 50
**Table 11.** The results of QuickBird XS images..... 51
**Table 12.** For QuickBird XS image the grouping of test fields based on their accuracy values..... 54
**Table 13.** The results of QuickBird PS images..... 56
**Table 14.** For QuickBird PS imagery the grouping of test fields based on their accuracy values..... 59
**Table 15.** The results of Spot5 XS images..... 60
**Table 16.** For Spot5 XS image the grouping of the test fields based on their accuracy values..... 63
**Table 17.** The comparison of the grouping of the test fields based on their accuracies ..... 64

# LIST OF FIGURES

Page

**Figure 1.1.** The graphical user interface designed for the implementation of the proposed marker controlled watershed segmentation method ..... 5

**Figure 1.2.** The illustration of the implementation of the developed method on test Field #6 using the Ikonos (XS) image and the result of accuracy assessment..... 5

**Figure 2.1.** Histogram thresholding [23] using Otsu's thresholding method..... 6

**Figure 2.2.** Segmentation of image by using edge information [26]. ..... 7

**Figure 2.3.** Segmentation by fusion of histogram-based K-means clustering in different color spaces [40] ..... 9

**Figure 2.4.** An example for region growing segmentation ..... 10

**Figure 3.1.** The proposed image segmentation method ..... 14

**Figure 3.2.** (a) True color representation of the Ikonos XS image for test Field #6, and (b) the result of Intensity transformation ..... 16

**Figure 3.3.** (a) The intensity image of test Field #6 with the added Gaussian noise and (b) the implementation of a 3×3 mean filter ..... 17

**Figure 3.4.** (a) The intensity image of test Field #6 with the added Salt & pepper noise and (b) the implementation of a 3×3 median filter..... 18

**Figure 3.5.** Orthogonal gradient generation..... 19

**Figure 3.6.** The 3×3 sized mask ..... 20

**Figure 3.7.a** The Sobel horizontal mask ..... 20

**Figure 3.7.b** The Sobel vertical mask..... 20

**Figure 3.8.** (a) Field #6 intensity image. (b) Gradient magnitude of Field #6 ..... 20

**Figure 3.9.** Intensity histogram of the Field #7..... 21

**Figure 3.10.** Thresholding of the Field #7 image with the value of 51 that was obtained from the histogram..... 22

**Figure 3.11.** The result of the implementation of Otsu's method on Field #6 using the Ikonos image..... 24

**Figure 3.12.** Masking out of the 1st step thresholding from the original image..... 25

**Figure 3.13.** (a) The Ikonos image for Field #6 (b) The result of 1st step of Otsu thresholding, (c) The result of 2nd step of Otsu thresholding ..... 26

**Figure 3.14.** The structuring elements with different shapes and sizes ..... 27

**Figure 3.15.** The implemented structuring element in this study..... 27

**Figure 3.16.** Illustration of erosion ..... 28
**Figure 3.17.** Implementation of two structuring elements (b & f) on the image (a). ..... 28
**Figure 3.18.** The implementation of hole filling on Field #4 (a) The original binary image after Otsu thresholding with the holes that are shown by red circles (b) The result of hole filling operation on (a) ..... 29
**Figure 3.19.** Hole Filling using mathematical morphology [75] ..... 30
**Figure 3.20.** Implementation of Erosion on Field #6 (a) Output of second step of Otsu thresholding with the additional strips that are shown with the red circle (b) implementation of Erosion operation that eliminate the additional strips ..... 31
**Figure 3.21.** (a) Output of reversing step of Field #6 with the additional strips that shown with the red circle (b) implementation of Erosion operation that eliminate the additional strips ..... 32
**Figure 3.22.** Final foreground markers for Field #6..... 32
**Figure 3.23.** Watershed transform ..... 33
**Figure 3.24.** Watershed segmentation using the gradient. (a) A grayscale image of nuclei, (b) The gradient magnitude of (a), (c) Watershed transform of gradient image, (d) Applying a smoothing filter to gradient for overcoming the over segmentation, (e) Watershed transform of (d), and (f) is the colored representation of segmented objects ..... 34
**Figure 3.25.** Marker-controlled watershed segmentation. (a) Gray scale image of nuclei, (b) Gradient magnitude, (c) Watershed transform of gradient image, (d) Watershed ridge line of gradient, after applying a smoothing filter, (e) Marker image, (f) Watershed ridge lines, (g) Imposition of gradient and markers and watershed ridge lines, (h) Result of segmentation ..... 35
**Figure 3.26.** Comparison of geometries between reference fields and calculated fields for sample field..... 38
**Figure 4.1.** The location of study area in Turkey..... 39

# SYMBOLS AND ABBREVIATIONS

| | |
|---|---|
| FCM | Fuzzy C - Means |
| GEOBIA | Geographic Object-Based Image Analysis |
| GIS | Geographical Information System |
| GIScience | Geographical Information Science |
| GUI | Graphical User Interface |
| NDVI | Normalized Difference Vegetation Index |
| NIR | Near Infra-Red |
| OBIA | Object Based Image Analysis |
| PS | Pan Sharpened |
| RAG | Region Adjacency Graph |
| SE | Structuring Element |
| SOFM | Self-Organized Feature Maps |
| SRG | Seeded Region Growing |
| UTM | Universal Transverse Mercator |

# 1. INTRODUCTION

Producing food and the cost of food production are quite important for every country. Because of this, “agriculture” is one of the most significant factors in the economy of every country. In developing countries, in line with the quick increase of urban population, the need for food production is increasing. Therefore, the agriculture section needs to be more modernized in the monitoring section in order to make more effective decisions. The decisions to be taken are important for governmental foundations and also for farmers.

Product estimation, mapping soil productivity, assessing the crop damage caused by disasters like storms and drought and monitoring the crop production statistics are of the sciences that serve to agricultural purposes. Mapping and recognition of the crop fields help these sciences about the agricultural yields.

Farmers’ statements and/or ground visits of the fields are the traditional methods of gathering up-to-date information about the agriculture fields. However, because of time and cost aspects and also inaccurate declarations traditional methods are inefficient.

Remote sensing is a valuable tool for agricultural studies. To be precise, spaceborne imagery can be used as a powerful way for specifying, locating and classifying agricultural areas, controlling their changes in time over large areas and collecting crop production statistics for decision markers.

Automatic image classification of remotely sensed images is the most habitually used technique for detecting the crop fields. For a very long time, the common pixel-based classification has been used as the major method of image classification. Recently, object-based classification (also called as field-based or polygon-based), a new way of image classification, has been developed. The recent research studies have proven the advantage of the object-based classification method over the traditional (pixel-based) method. Pixel-based methods try to label each pixel exclusively, taking into account the pixel as the main aspect [1]. These methods can cause different errors in the classification process. Object-based classification is employed to overcome the pixel-based method’s limitations. Object-based classification methods focus on the groups of pixels (segments) that create an object as the main aspect and try to label the objects and all the pixels that fall within the

objects. Object-based (or better to say field-based classification for this study) provides considerably more accurate results in comparison with the pixel-based methods [2] and [3]. This is because, this method focuses not only on spectral properties of the objects, but also on their orientation, shapes and adjacency to other objects.

In field-based image classification, segmentation is the initial and an important step of the procedure, through which the homogenous areas in the image are determined. Object-based image analysis (OBIA) [4] is a rising field that aims to extract complex information by image processing. OBIA was to be considered as a sub-discipline of GIScience as proposed by [5] and is now referred to as GEOBIA [5]. In most of the GEOBIA literature, researchers try to come up with efficient segmentation methods to use in GEOBIA [6], [7] and [8]. Many different segmentation methods have been developed over the years [9], [10], [11] and [12].

Image segmentation algorithms can be divided to three generic types as edge-based, region-based and hybrid methods. Edge-based methods are based on separating the objects by finding edges between neighboring pixels [13]. This method attempts to find the objects or field boundaries and then locate the objects themselves by filling the boundaries. Region-based segmentation methods operate as ‘region growing’ or ‘region split and merging’ [14]. The combination of the edge-based and region-based methods are the hybrid methods [7], [15] and [16]

Looking at the agricultural satellite images, it can be seen that there exist various objects in addition to agricultural fields. This is an important problem for segmenting the whole image because the segmentation algorithm should deal with the other elements and objects such as ditches, roads and streams, which do not belong to any of the crop fields. Hence, in order to remove or reduce the efficiency of the additional objects in the image, a prior knowledge about the permanent boundaries defined by the roads, ditches, channels, etc. have become significant. This prior knowledge is now available in most countries as digital topographic database stored in a geographic information system (GIS). Thus, in this thesis, an approach is presented for the automatic extraction of agricultural fields confined by the permanent boundaries defined by the roads, channels, ditches, rivers, etc. stored in a GIS database. The tests of the proposed method were carried out in the test fields selected in an agricultural area, located near Karacabey, Bursa located in north-

west of Turkey. The satellite images used in the tests include the Ikonos multispectral (XS) image acquired on 15 July 2004, the SPOT5 multispectral (XS) image acquired on 22 July 2004, the QuickBird multispectral (XS) and the QuickBird Pansharpened (PS) images acquired on 13 August 2004.

### 1.1. The Thesis' Goals

The goals of this thesis are as follows:

- To develop an automatic field-based image segmentation method for extracting the agricultural fields confined by the permanent boundaries defined by the roads, channels, ditches, canals, etc.
- To assess the compatibility of Otsu's thresholding method for providing the proper foreground markers for using in a marker controlled watershed segmentation algorithm.
- To evaluate the suitability of marker controlled watershed segmentation to extract agricultural fields.
- To analyze the advantages and disadvantages of the proposed method on the obtained results.
- To achieve an accurate segmented image for improving the accuracy of field-based classification techniques.

### 1.2. Contributions

The first and major contribution of this thesis is the development of an approach that utilizes both the Otsu and watershed segmentation methods to extract agricultural fields confined by the permanent boundaries defined by the roads, channels, ditches, rivers, etc. The second contribution of the study is the development of an iterative segmentation method which makes use of Otsu's segmentation algorithm to prepare the markers for the watershed segmentation method. The final contribution of the thesis is the development of an automatic marker controlled watershed algorithm that operates on the output of Otsu's segmentation method.

### 1.3. Thesis Outline

The rest of the thesis is organized in four chapters. Chapter 2 illustrates a brief review of the method for operating the field-based image segmentation and the watershed algorithm. Chapter 3 explains the proposed methodology named "Automatic Segmentation of High Resolution Satellite Images into Agricultural Fields Using Improved Watershed Segmentation". In chapter 4, the data sets and the results are described and the crucial discussion of implementing the proposed method on the test fields is presented. Finally, in chapter 5, the conclusions and recommendations for future research are given.

### 1.4. Software

To implement the developed methodology in test areas, a program was developed in MATLAB programming environment. Using this program, all the necessary processing and analysis operations are carried out. These include transforming an RGB image into an intensity image, calculating a gradient magnitude image from the intensity image, obtaining initial markers for watershed segmentation by using the Otsu's thresholding method and implementing a marker controlled watershed segmentation algorithm.

In addition, a graphical user interface (GUI) was designed in MATLAB programming environment. This interface makes the developed methodology easy to use. As it is shown in Figure 1.1, the original image can be loaded by pressing the 'Browse Original image' button. After loading the image, the program requests to enter the size of the average and median filters. After defining the filter size, the image is segmented upon pressing the 'Segmentation' button. Further, the accuracy assessment operation can also be carried out using this interface. This is accomplished using the 'Browse Reference Image' button for loading the reference image and the 'Accuracy Assessment' button for showing the results, as it can be seen in Figure 1.2.

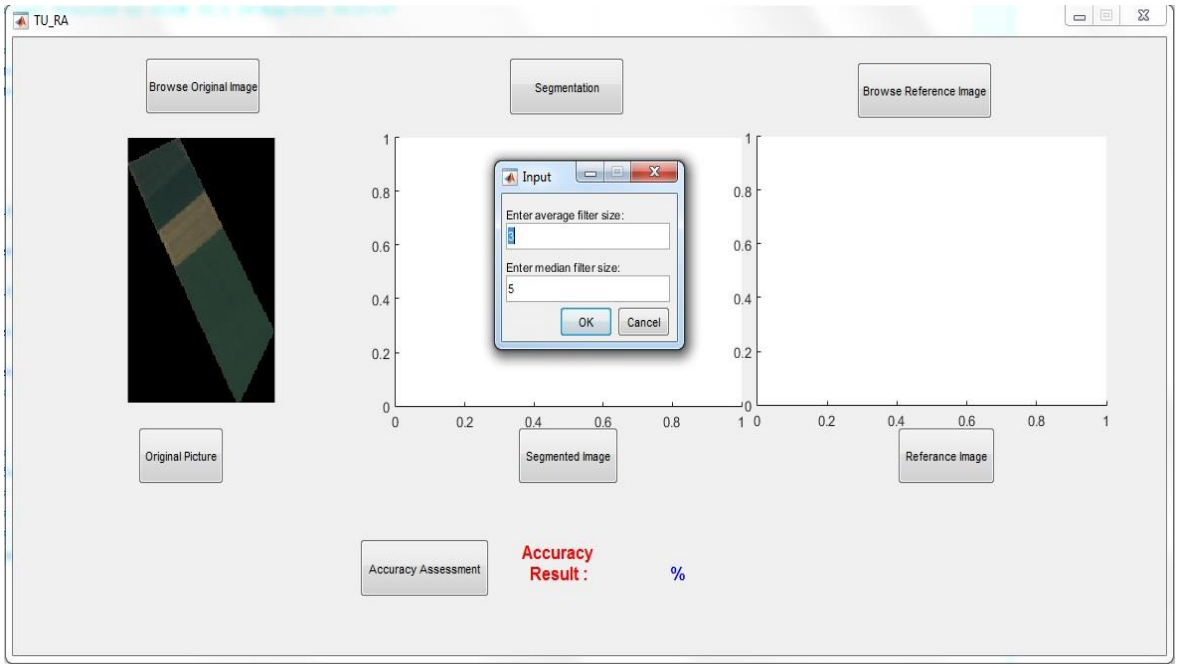


**Figure 1.1.** The graphical user interface designed for the implementation of the proposed marker controlled watershed segmentation method

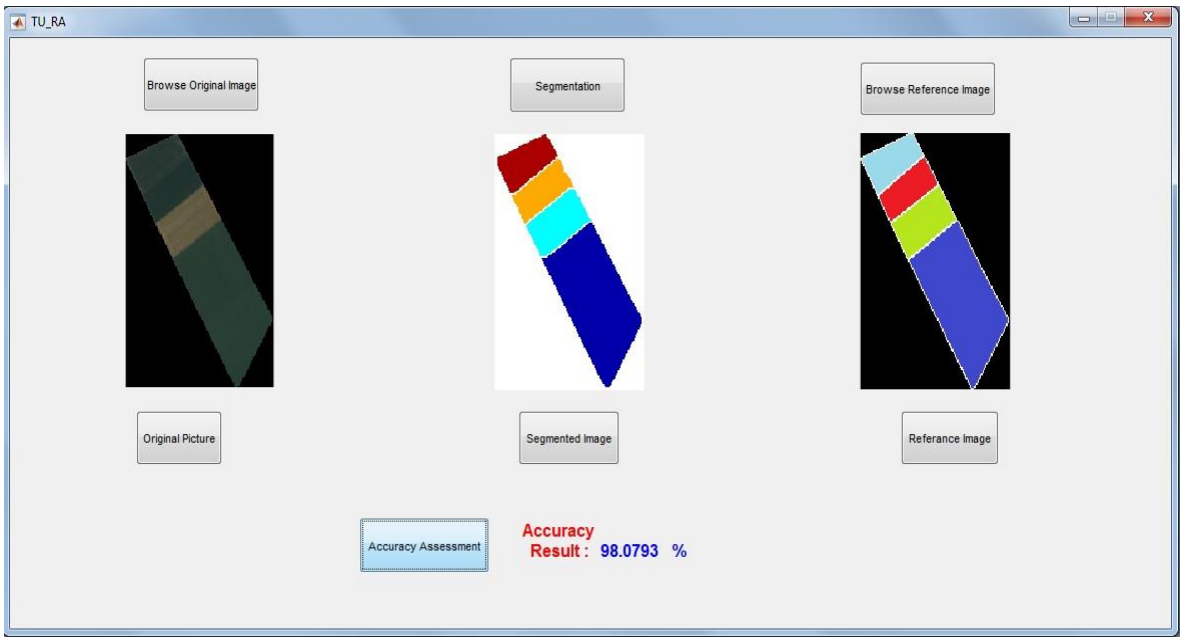


**Figure 1.2.** The illustration of the implementation of the developed method on test Field #6 using the Ikonos (XS) image and the result of accuracy assessment

# 2. LITERATURE REVIEW

## 2.1. Image Segmentation

There are various techniques for employing image segmentation. Most of these techniques make use of one or a combination of approaches based on: i) histogram thresholding, ii) edge detection, iii) tree/graph analysis, iv) clustering, v) probabilistic/Bayesian models, vi) neural networks and vii) region growing [17].

Histogram thresholding or simply thresholding is the most simple but effective method for image segmentation. Separating the objects and background into without overlapping sets is the purpose of thresholding operation. A review of thresholding methods and their applications can be found in [18]. The minimum error thresholding method, which was proposed by [19], tries to find the optimum threshold by optimizing the average pixel classification error rate directly. A thresholding technique, which is very helpful for segmenting the outdoor color images, was proposed by [20]. In this method, the image is thresholded at the histogram's most well separated peak. Another thresholding approach was proposed by [21] in the area of document images. This method, which is based on divider analysis, segments the brightest uniform object and leaves the darkest homogeneous object. One of the famous and effective thresholding methods, which was also used in this study, is Otsu's thresholding method. This method utilizes diacritical analysis to find the maximum separability of classes [22]. Figure 2.1. illustrates an example of histogram thresholding using Otsu's thresholding method.

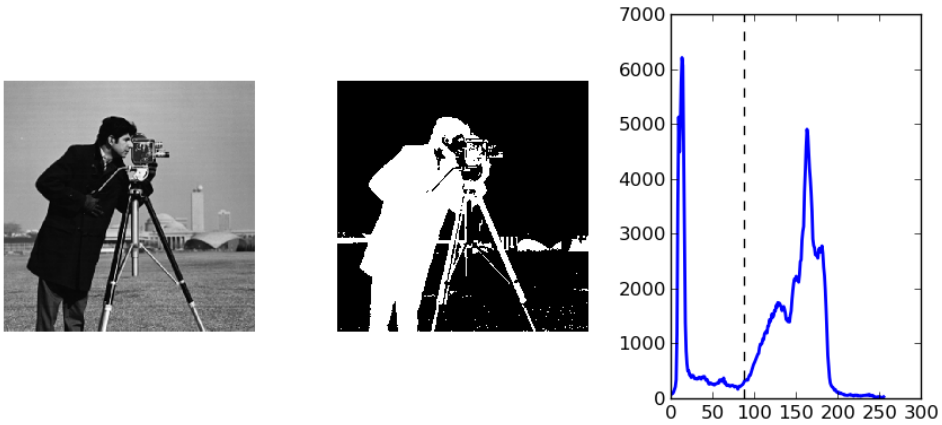


**Figure 2.1.** Histogram thresholding [23] using Otsu's thresholding method

Edge detection methods try to carry out the image segmentation through boundary analysis. A good number of algorithms for locating the boundaries of an object correctly in an image, proposed by [24]. First, smoothing and noise-removal operations are performed to clean up the raw data. Then, the edge representation is generated. For finding the edge-strength at each point, differentiation is done in the image [24]. To remove multiple edges established by spatial differentiation of boundaries, suppression is carried out. Third, the edges are joined into line segments and features are computed. Length, contrast, frequency, mean, variance and location of each line segment are of the computed features. Finally, post-processing is carried out to remove unwanted line segments. The output of the method is a set of line segments with a list of attributes, such as length and confidence[24].

The edge based segmentation is not very successful because of small gaps that allow merging of dissimilar regions [17]. An expansion-contraction technique in which edge regions are expanded to close gaps and then contracted after the separate regions have been labeled proposed by [25], in order to avoid these problems. The size of expansion is controlled such that small regions are not absorbed by this process. The process includes the use of Sobel filter for finding edge strengths and directions at every point. The ridge lines will remain as the result after applying a skeleton operation to the edges. The ridges separate different objects but there may be small gaps. By expanding active edge regions, labeling the segmented uniform objects, and then contracting edge regions, the segmentation is performed [25]. An example of edge based method is shown in Figure 2.2.

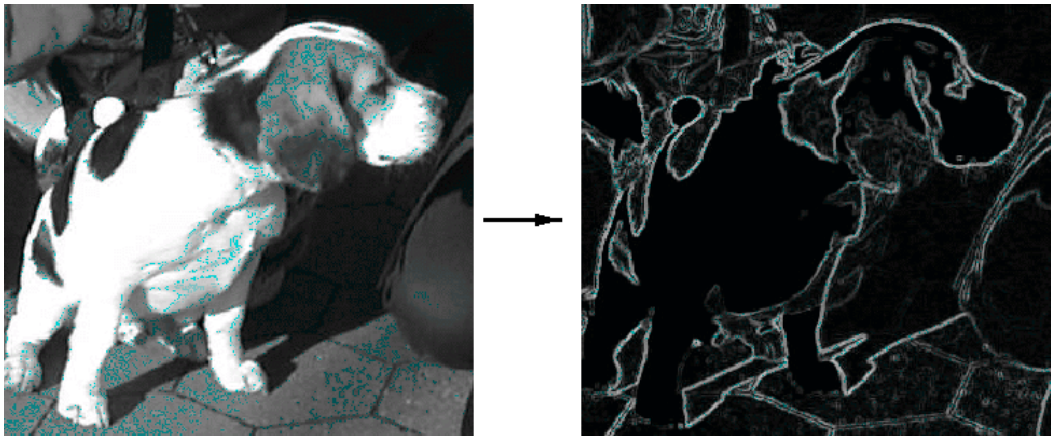

**Figure 2.2.** Segmentation of image by using edge information [26].

Tree/graph analysis was proposed by [27] as a new method for segmentation, which is taken from the unity of a set of different segmentation outputs on one input image. The spatial combination of the local neighborhood of a pixel, for every pair of adjacent pixels their collected statistics are used for determining local homogeneity, instead of statistics characterizing. Several initial segmentations are derived from the same input image by changing the probabilistic component of the hierarchical Region Adjacency Graph (RAG) pyramid based technique[17]. From the combination of these initial segmentations, for every adjacent pixel pair, a co-occurrence probability is calculated, which takes global information (about the image) at the local pixel level. The final segmentation of the input image is carried out by processing the co-occurrence probability field with the same RAG pyramid technique. Based on the combination about local homogeneity, the pixel pairs with high co-occurrence probability are grouped together. This technique can also be used to extract the high trust homogeneous regions from the co-occurrence probability field.

Clustering is another method for image segmentation. It is the process of dividing an image into natural groups such that the same group contains pixels with similar values while the pixels in different groups are dissimilar to each other [28], [28], [29] and [30]. Cluster analysis divides the data in to significant segments and it can be applied for image segmentation or classification purposes. Clustering is widely used in a range of applications such as image segmentation and can be considered as the most important unsupervised learning [31]. K-means is one of the simplest clustering algorithms [32] and [33]. This method tries a simple way for classifying an image into a certain number of clusters (assume k clusters) [34] and [35]. An improvement was made on the k-means method by [36] and [37]. Fuzzy c-means (FCM) is another method for clustering. This method allows to a part of data to belong to two or more clusters [36] and [37]. In other words, this method let the pixels belong to multiple classes with changing degree of membership. An improvement was made on FCM algorithm by [38] based on the data compression concept which reduces the dimensionality of the input data. Another important issue for study is the validity of clusters. Assessment of several areas of clustering methodology including the description of clusters, definition of the number of clusters, exploratory partitional clustering algorithms and the effect of noise on

defining accurate clusters were proposed by [39]. Cluster reliability criteria including maximum likelihood information criteria and sum of squared errors are discussed in [39]. Figure 2.3 illustrates an example of segmentation by fusion of histogram-based K-means clustering in different color spaces.

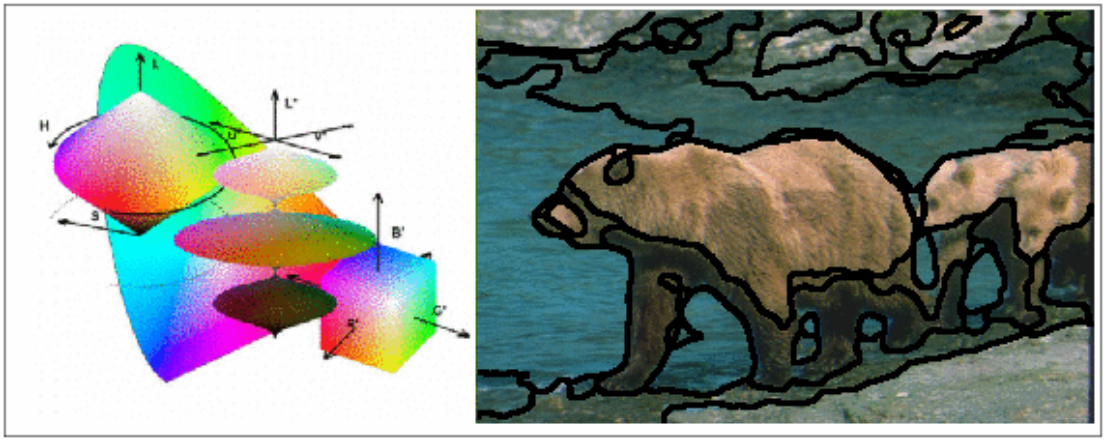

**Figure 2.3.** Segmentation by fusion of histogram-based K-means clustering in different color spaces [40]

Probabilistic/Bayesian models is another method for image segmentation. An image segmentation method was examined by unifying region and boundary information using the co-occurrence matrices [41]. The feature space were generate by using the co-occurrence matrices. The context of an ensemble of images were used to perform the analysis. Initial segmentation was done by locating the intensities of each pixel and its neighbors in the co-occurrence matrix. Each pixel was then related with a tuple pixels which specifies whether it belongs to a given object or if it is a boundary pixel. This experimental segmentation approach was then carried out by relaxation labelling that ensures local stability of pixel labelling during segmentation by minimizing the entropy of local neighborhoods. If a pixel does not fit to the boundary, then it is assigned to one of the objects. The stability for objects and boundary was obtained assuming that boundaries are not wider than one pixel.

Neural networks have also been proposed as another automatic segmentation method. [42] and [43] have developed the procedure of image segmentation using Self-Organizing Feature Maps (SOFM). The use of these neural network samples is thought-out tantamount to multi thresholding where the output of the network describes a number of homogeneous clusters [17].

Region growing algorithms take one or more pixels, called seeds or markers, and grow the regions around them based upon a certain homogeneity criteria. If the adjoining pixels are similar to the marker, they are merged with them within a single region. The process iterates until all the pixels in the image are specified to one or more regions. For region growing, markers can be automatically or manually selected. Automatic selection of markers can be based on finding pixels that are of interest, e.g. the brightest pixel in an infra-red image can be considered as a marker pixel. They can also be specified from the peaks found in an image histogram. On the other hand, markers can also be selected manually for every object present in the image [17]. An effective example of "Region Growing" by using marker controlled watershed algorithm is shown in figure 2.4.

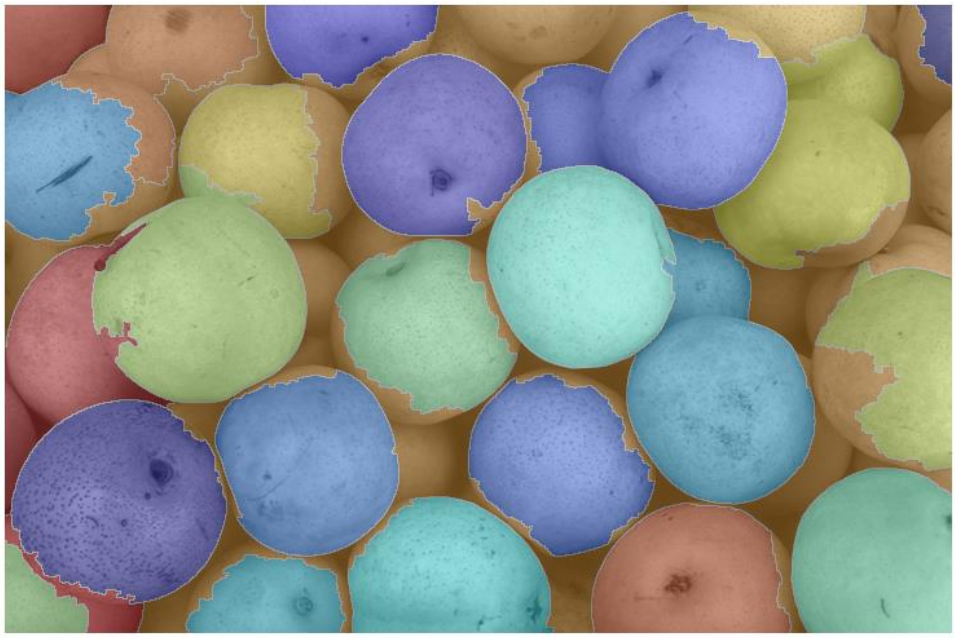

**Figure 2.4.** An example for region growing segmentation

Two of the most representative algorithms of this approach are the Seeded Region Growing (SRG) [17] and the Watershed Transformation based algorithms [44], along with their variations. As watershed algorithms were employed for the present work, it is described below.

## 2.2. The Watershed Algorithm

The watershed transform, which is a region-based approach, was originally developed by [45] and later improved by [46].The main idea of watershed comes from a topographic analogy, in which the watershed lines divide individual catchment basins. An image can be considered as a topography where the gradient image pixel values represent altitudes. The edges of the regions that correspond to high watersheds and low interiors refer to catchment basins. The surface in a catchment basin is homogeneous, in the sense that all pixels that fall within the same catchment basin are connected with the basin's local minima. The catchment basins represent the segmented image.

There exist a number of different algorithms to compute watershed transform, however most of them fall into two classifications. In the first class of algorithms, the pixels are associated with catchment basins based on their shortest topological distance from local minima. In the second class, suppose that holes are pierced at every regional minima and the image surface is dipped into water. The water will then flood the areas adjacent to regional minima. As the image is continued to be immersed, some of the flood areas (catchment basins) will be merged. When two or more flood areas are merged, watershed lines are drawn between them. Hence, the resulting watershed lines define the desired segmentation result.

The watershed transform, is a powerful method of choice for image segmentation [47]. Morphology watershed transform is a powerful morphological method for image segmentation. Image segmentation based on watershed transformation can establish more accurate segmentation results with low computational costs [48]. Watershed transformation has various applications for different types of images. An application of watershed algorithm was used for road segmentation by [49] and [50]. [51] and [52] applied watershed transform for building extraction. Another application of watershed by [53] was used for agricultural field detection. Watershed transformation had also a wide use in medical image segmentation [54], [55], [56].

Still, inasmuch as watershed transform is basically a greyscale transformation based on pixel values and their order relation in a greyscale image, its application for the segmentation of multispectral images is not so common [57], [58], [59], [60] and [61].

One of the problems of watershed transformation is over-segmentation. Therefore in this study, to prevent the over-segmentation problem and also for the reason of the precision, the marker controlled watershed method is used [62].

### 2.3. Marker Controlled Watershed

The watershed transform algorithm is a popular segmentation method, as it is computationally effective and does not need any parameter [63]. However, the application of watershed algorithm is greatly influenced by the noise and other local irregularities in the image [64]. This leads to over-segmentation of regions to an extent that the segmented image itself looks like a noisy image. To increase the accuracy of the results and to compensate watershed methods' limits, a prior knowledge that often consists in the number and the positions of the regions through the definition of some markers can be considered for applying the marker-based watershed [63]. The marker controlled watershed is the most famous and widely used enhancement of the watershed transform [62]. Various descriptions have been given in the literature, [65], [66] and [67], for showing the improvement of the markers on the watershed algorithm.

# 3. METHODOLOGY

In this chapter, the method used is described. The main steps followed for the developed method are shown in Figure 3.1. These steps include: (i) Preprocessing, (ii) Initial segmentation, and (iii) Final segmentation.

In the preprocessing step, the original Red, Green, and Blue (RGB) bands are transformed to an intensity image. Then, the generated intensity image filtered using the low pass mean and median filters. Next, the gradient magnitude is calculated from the low pass filtered intensity image.

In the second step, which is initial segmentation, first the intensity image is segmented using the Otsu Thresholding segmentation method. Then, the morphological operations applied to the segmented image. After that, the Otsu Thresholding segmentation procedure is applied for the second time.

In the final step of the developed method the watershed segmentation is applied on the outputs of the two previous steps (The gradient magnitude and the output of Otsu thresholding).

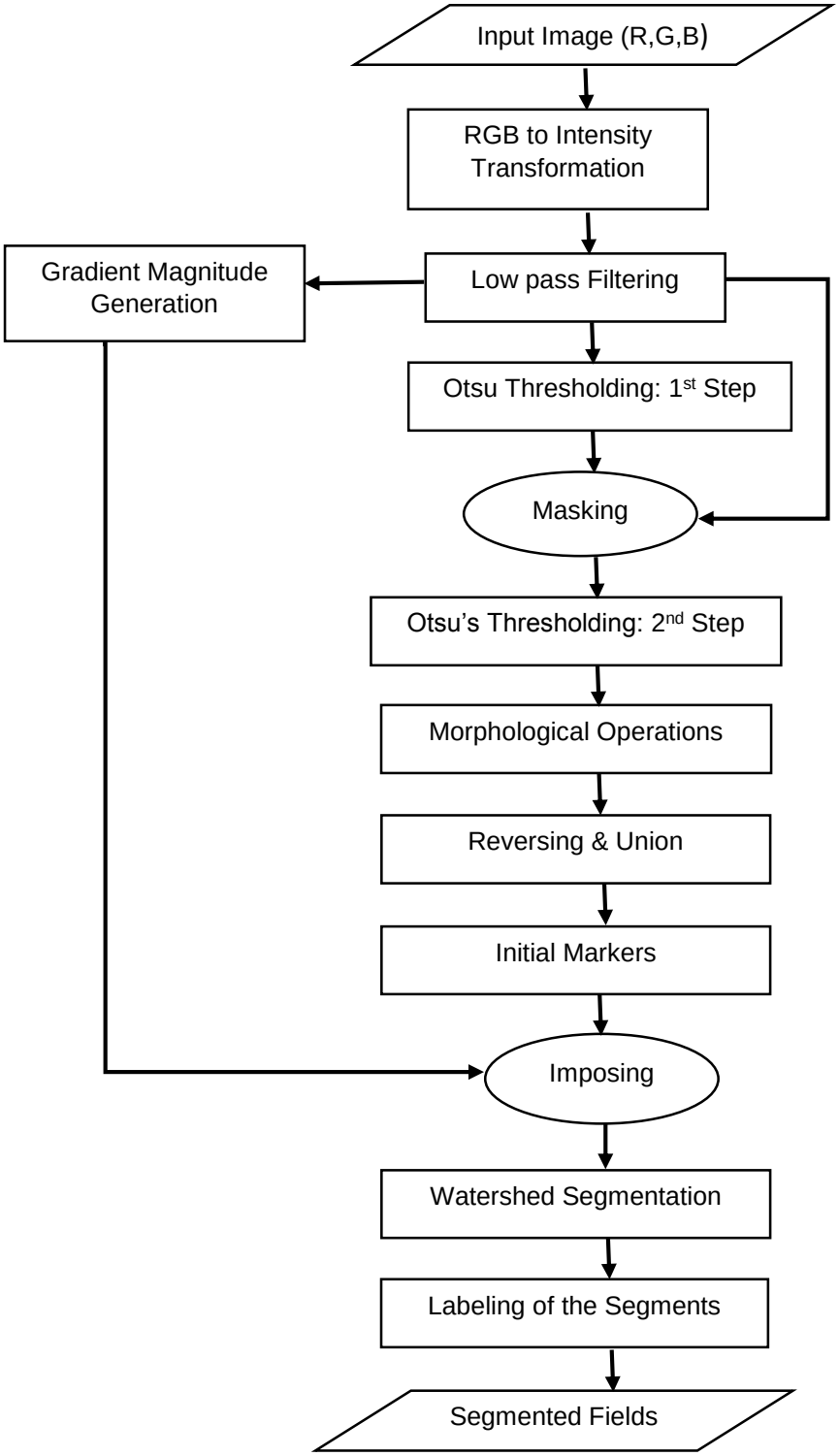


**Figure 3.1.** The proposed image segmentation method

### 3.1. Preprocessing

#### 3.1.1. RGB to Intensity Transformation

Intensity is one of the HSI (Hue, Saturation and Intensity) color space components. In this color representation, the “I” component, stands for intensity which represents the average gray level. For the transformation of RGB to HSI, first the RGB values are transformed into Y, C1 andC2 values using Eq. 3-1 [68] :

$$\begin{bmatrix} Y \\ C1 \\ C2 \end{bmatrix} = \begin{bmatrix} 1/3 & 1/3 & 1/3 \\ 1 & -1/2 & -1/2 \\ 0 & -\sqrt{3}/2 & -\sqrt{3}/2 \end{bmatrix} . \begin{bmatrix} R \\ G \\ B \end{bmatrix} \tag{3-1}$$

Then, the HSI values can be computed as:

$$\text{I = Y , S = } \sqrt{C_1^2 + C_2^2}$$

$$\text{H = } \begin{cases} Arc\cos(C_2/S) & C_1 \geq 0 \\ 2\pi - Arc\cos(C_2/S) & C_1 \geq 0 \end{cases} \tag{3-2}$$

As it can be seen in the flowchart, in Figure 3.1, for watershed segmentation, the intensity image is required. So Eq. 3-1 and 3-2 can be summarized as:

$$Intensity = \frac{R + G + B}{3} \tag{3-3}$$

In this study, the intensity image is generated from the RGB bands of the original image using equation (3.3) and further processing operations are carried out using the intensity image. For a selected test field (Field #6) used in this study, the result of the Intensity transformation as performed on the Ikonos satellite image is shown in Figure 3.2.

a b

**Figure 3.2.** (a) True color representation of the Ikonos XS image for test Field #6, and (b) the result of Intensity transformation

### 3.1.2. Smoothing Spatial Filters

Filtering is a major operation in image processing. It can be used for image enhancement, noise removal, edge detector and image sharpening. At the spatial domain, filtering is a pixel neighborhood operation. The widely used smoothing spatial filters include average, median, and, Gaussian. The smoothing filters normally have the effect of noise reducing and are also called “Low Pass Filters”.

#### 3.1.2.1. Average Filter

The most popular smoothing linear filter is the “Average (Mean) Filter”. This filter gets its output value from the mean of its neighborhood pixels value. Thus, the filtering mask is like below (3×3 example):

$$h = {}^{1}/_{9}\begin{bmatrix}1 & 1 & 1\\ 1 & 1 & 1\\ 1 & 1 & 1\end{bmatrix} \qquad (3\text{-}4)$$

In application, the size of the mask, controls the amount of smoothing and detail loss. The result of applying this filter on an image will be an image with reduced “sharp” shifts in gray levels. The most noticeable application of this filter is noise removing. For example, the result of applying mean filter is shown below in Figure 3.3. (The size of the mask is 3×3)

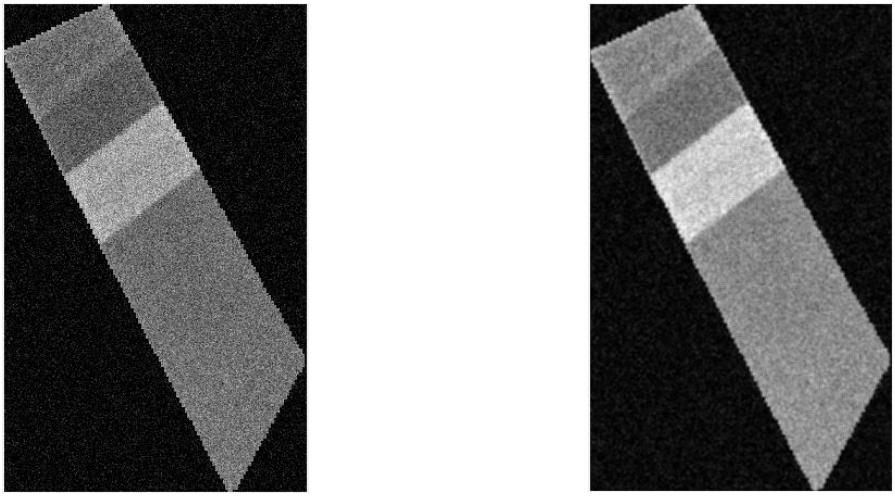

a b

**Figure 3.3.** (a) The intensity image of test Field #6 with the added Gaussian noise and (b) the implementation of a 3×3 mean filter

### 3.1.2.2. Median Filter

This filter, replaces the value of a pixel by the median of the gray levels in the neighborhood of the main pixel in the filter window. In order to apply the median filter at a point in an image, the pixel value of interest and its neighbors in the filter window are sorted and the main pixel value is replaced by the determined median value. For example, in a 3×3 window size neighborhood, the median is the $5^{th}$ largest value and in a 5×5 neighborhood, it is the $13^{th}$ largest value and so on.

This filter is famous for its great noise-removing abilities that it provides against certain types of random noises, with far less blurring than linear smoothing filters of the same mask size. Median filters are especially effective against the impulse noise, also called salt-and-pepper noise [69]. The effect of median filter is shown in Figure 3.4.

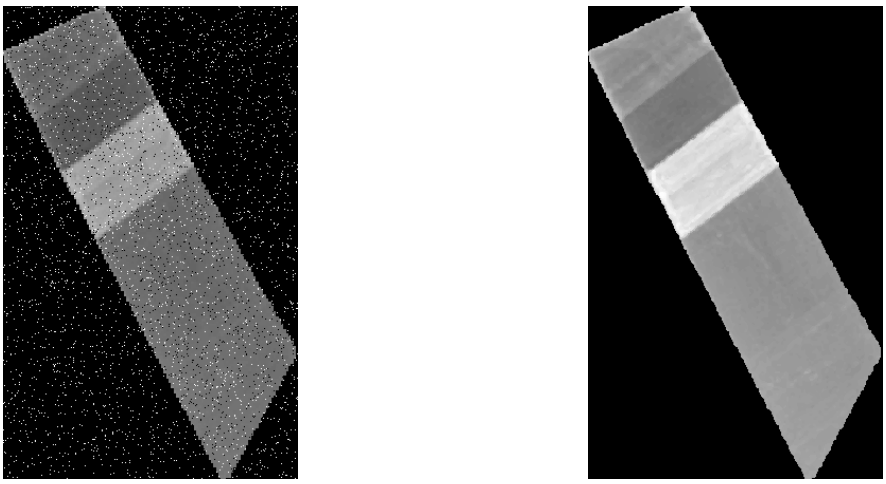

a b

**Figure 3.4.** (a) The intensity image of test Field #6 with the added Salt & pepper noise and (b) the implementation of a 3×3 median filter

### 3.1.3. Image Gradient

The gradient of an image is the directional change in the intensity in the image. The gradient carries two kinds of information: The magnitude of the gradient, which shows how rapidly the image is changing, and the direction of the gradient, which shows the direction of the quick changes. To interpret this situation, imagine an image as a terrain that has height, instead of the intensity at each point. For any point on this terrain, the direction of uphill is the direction of the gradient, and the rate of height changing per taking a very small step uphill is the magnitude of the gradient.

The gradient of a function $f(x,y)$ at coordinate $(x,y)$ is characterized as two-dimensional vector:

$$\nabla \mathbf{F} = \begin{bmatrix} g_x \\ g_y \end{bmatrix} = \begin{bmatrix} \dfrac{\partial f}{\partial x} \\ \dfrac{\partial f}{\partial y} \end{bmatrix} \tag{3-5}$$

This vector points in the direction of the highest rate of change of $f$ at location$(x,y)$. The magnitude (length) of this vector is computed as:

$$\nabla f = mag(\nabla \mathbf{F}) = \left[g_x^2 + g_y^2\right]^{\frac{1}{2}}$$

$$= \left[\left(\partial f/\partial x\right)^2 + \left(\partial f/\partial y\right)^2\right]^{\frac{1}{2}} \quad (3\text{-}6)$$

Sometimes, this value is approximated by the absolute values:

$$\nabla f \approx |g_x| + |g_y| \quad (3\text{-}7)$$

It is customary to calculate the gradient by taking the differences of the intensity values over small neighborhoods in an image. The 3×3 sized mask, which is shown in Figure (3.6.), is the example neighborhood, in which m's illustrate the gray-scale values. This method is also called "Orthogonal Gradient Generation"[70]. Figure (3.5) describes how the orthogonal gradient generation is generated.

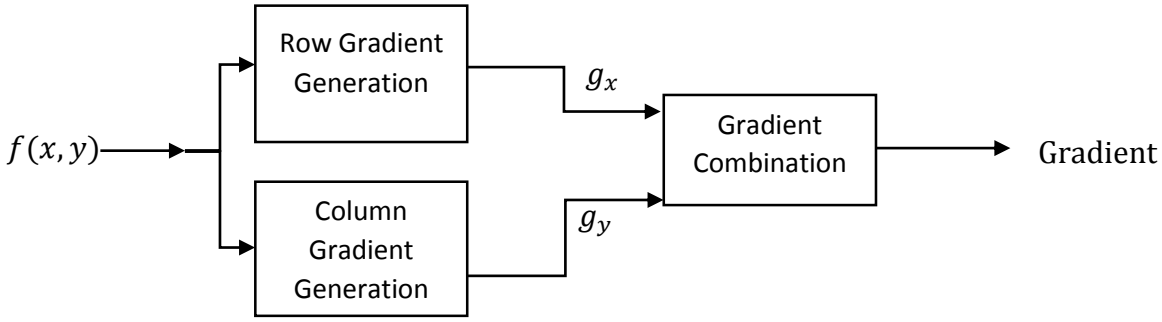


**Figure 3.5.** Orthogonal gradient generation

The gradients in x (vertical) and y (horizontal) directions at the center point are given by:

$$g_x = (m_7 + 2m_8 + m_9) - (m_1 + 2m_2 + m_3) \quad (3\text{-}8)$$

$$g_y = (m_3 + 2m_6 + m_9) - (m_1 + 2m_4 + m_7) \quad (3\text{-}9)$$

These two values are computed for all pixels in an image by filtering the image independently with two masks. In this study, the Sobel masks, which are shown in Figures 3.7.a &.b, are used in x and y directions. Then, by summing the absolute

values of the two filtered images, the desired gradient image is obtained. The gradient magnitude computed for a selected test Field #6 is shown in Figure 3.8.

| | | |
|---|---|---|
| $m_1$ | $m_2$ | $m_3$ |
| $m_4$ | $m_5$ | $m_6$ |
| $m_7$ | $m_8$ | $m_9$ |

**Figure 3.6.** The 3×3 sized mask

| | | |
|---|---|---|
| **-1** | **-2** | **-1** |
| **0** | **0** | **0** |
| **1** | **2** | **1** |

**Figure 3.7.a** The Sobel horizontal mask

| | | |
|---|---|---|
| **-1** | **0** | **1** |
| **-2** | **0** | **2** |
| **-1** | **0** | **1** |

**Figure 3.7.b** The Sobel vertical mask

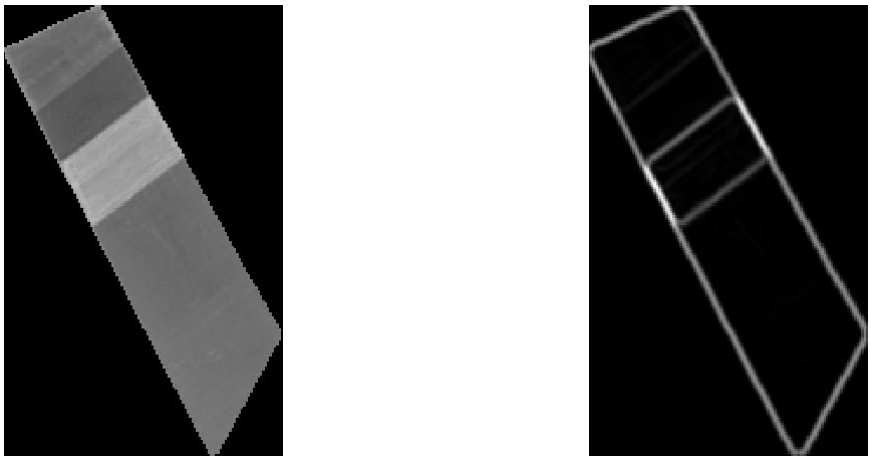

a b

**Figure 3.8.** (a) Field #6 intensity image. (b) Gradient magnitude of Field #6

### 3.2. Inner Segmentation

#### 3.2.1. Image Thresholding

##### 3.2.1.1. Fundamentals of Image Thresholding

Thresholding is a popular and simple technique for image segmentation. Lots of objects are characterized by constant reflection or light absorption of their surface. A properly determined threshold value can segment the objects and the background of the image. This method is so low-cost and fast and it is the oldest method for segmentation, but it is still widely used in simple applications. A thresholded image $g(i,j)$ is defined as:

$$g(i,j) = \begin{cases} 1 & for\ f(i,j) \geq T \\ 0 & for\ f(i,j) < T \end{cases} \quad (3\text{-}10)$$

Where $T$ is the threshold, $g(i,j) = 1$ stands for the objects and $g(i,j) = 0$ stands for the background elements. Imagine that the gray-levels histogram shown in Figure (3.9) corresponds to an image $f(i,j)$. The way to extract the objects from the background is to select the optimal threshold $T$ that separates the histogram. Any pixel$(i,j)$, for which $f(i,j) \geq 1$ (e.g. $T = 51$) is called an object pixel, otherwise, it is called a background pixel.

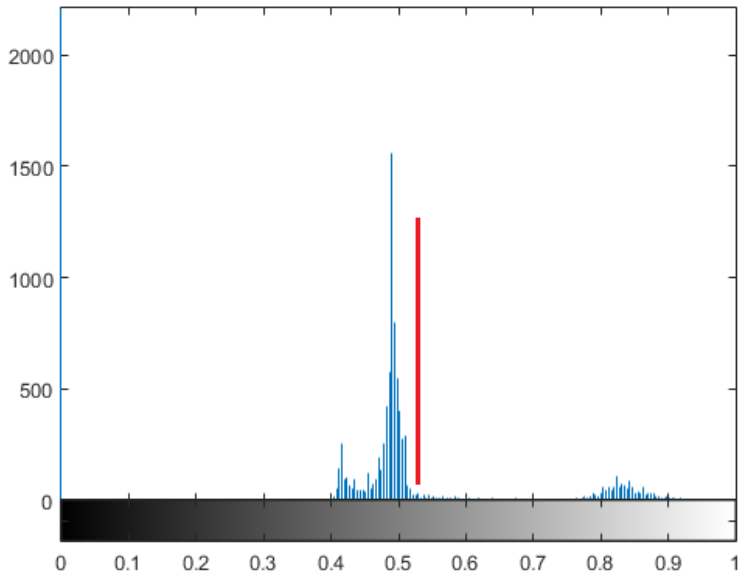


**Figure 3.9.** Intensity histogram of the Field #7

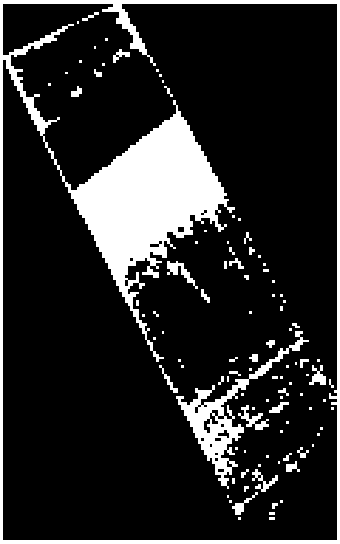

**Figure 3.10.** Thresholding of the Field #7 image with the value of 51 that was obtained from the histogram

### 3.2.1.2. Optimum Global Thresholding Using Otsu's Method

Thresholding which is viewed as a statistical decision theory problem, is objective to minimize the mean error that incurred in earmarking pixels to two classes.

In the present case, we use the Otsu's method for the preliminary segmentation operation[22]. This method is optimum in meaning that it maximizes the across-class variance, a famous measure used in the statistical divider analysis. The fundamental of this method is to make fine-threshold classes that are distinct with respect to their pixels intensity values and conversely, an optimum threshold that, in term of intensity, giving the good separation between the classes. Another property of this method is dependence of it, completely, to the calculations on the image histogram.

Let $q = [0,1,2,\dots,L-1]$ denote the gray-levels in an image with the size of $M \times N$ pixels, where $L$ represents the maximum number of gray-level in the image. Then, $Pq$ the component of the image histogram is computed as:

$$Pq = \frac{n_q}{n} \tag{3-11}$$

Where, $n$ is the total number of pixels and $n_q$ is the number of pixels with gray-level $q$. Assume that $k$ is chosen as a threshold and using it to threshold the input image

into class $C_1$ which is the set of pixels with gray-levels $[0,1,2,\dots,k]$ and $C_2$ which is the set of pixels with $[k+1,\dots,L-1]$ gray-level values. Because of the nature of Otsu's method which chooses a threshold value that maximizes the between class variance ($\sigma_B^2(k)$), so:

$$\sigma_B^2(k) = P_1(k)[m_1(k) - m_G]^2 + P_2(k)[m_2(k) - m_G]^2 \tag{3-12}$$

Where, $P_1(k)$ and $P_2(k)$ are the probabilities of occurring classes $C_1$ and $C_2$:

$$P_1(k) = \sum_{i=0}^{k} p_i \tag{3-13}$$

$$P_2(k) = \sum_{i=k+1}^{L-1} p_i = 1 - P_1(k) \tag{3-14}$$

Where, $m_1(k)$ and $m_2(k)$ represent the mean of gray-levels in class1 and class2 and $m_G$ stands for the mean of gray-levels of entire image:

$$m_G = \sum_{i=0}^{L-1} i p_i \tag{3-15}$$

By using the fact that, $P_2(k) = 1 - P_1(k)$ between class variance can be written as:

$$\sigma_B^2(k) = \frac{[m_G P_1(k) - m(k)]^2}{P_1(k)[1 - P_1(k)]} \tag{3-16}$$

In attention to the main idea of this method, the larger between class variance will lead to the well segment results. For finding the maximum of $\sigma_B^2(k)$, the all $L$ possible values of $k$ should be considered and the variance at each step should be calculated. The optimum value of $k$ is the value that gives the largest value of $\sigma_B^2(k)$. The average of all optimum $k$'s would be used if the maximum is not unique. The relation of $\sigma_B^2(k)$ with the image total gray-level variance is:

$$\eta(k) = \frac{\sigma_B^2(k)}{\sigma_G^2} \tag{3-17}$$

Where, $\eta(k)$ is the measure of the separability of the image gray-level values into two classes (Object & Background) and (it differs) in the range of $0 \leq \eta(k^*) \leq 1$, and $k^*$ is the optimum value of k. Constant images whose pixels' are fully inseparable, will be caused to the minimum value and the binary images whose pixels' are completely separable will be caused to the maximum value of this measure.

The implementation of this method can be summarized as following steps:

i. Normalization of image histogram by $p_i$
ii. Computing the cumulative sums, $P_1(k)$ and means, $m(k)$, for $k = 0,1, \dots, L-1$
iii. Obtaining $m_G$ by using Eq.3-15.
iv. Calculating the $\sigma_B^2(k)$ for $k = 0,1, \dots, L-1$
v. Obtaining the optimum value, $k^*$
vi. Calculating the separability measure,$\eta^*$, by evaluating Eq.3-17, for $k = k^*$.

### 3.2.2. First Step of Otsu Thresholding

In the final segmentation operation used in this study, which is watershed segmentation, one of the major steps is to find the foreground markers. Therefore, the Otsu's method is used to solve this problem. By means of applying Otsu's method iteratively, the desired foreground markers are obtained. The iterative Otsu will be explained later in this chapter, in sections 3.2 (2nd step of Otsu) and 3.4 (final step of Thresholding). Figure 3.11 illustrates the result of Otsu's method as applied to Field #6 using the Ikonos image.

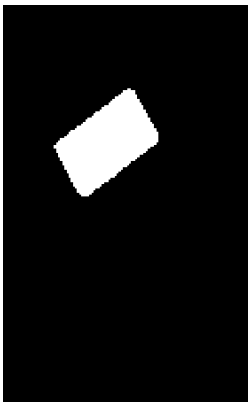

**Figure 3.11.** The result of the implementation of Otsu's method on Field #6 using the Ikonos image

### 3.2.3. Second Step of Otsu Thresholding

As mentioned earlier, in this study, the Otsu's Thresholding method is used to extract areas for seeding the markers to be used to perform watershed segmentation. In the first step of Otsu Thresholding, the results are not even close to the proper markers. This can be seen in Figure 3.12. This is because of the nature of the images and the reflection values. Therefore, to reach the optimal markers, the Otsu Thresholding method is applied once more. However, this time, those areas of the image, which are segmented in the first step, are excluded from the thresholding operation by simply masking them out. Therefore, the second thresholding operation is carried out on the masked image. This is illustrated in Figure 3.12, where the black color area within the field was detected in the first thresholding operation using Otsu and thus it is masked out in the second thresholding stage. By doing this, the area remains after the first thresholding operation using Otsu is reduced and therefore the second thresholding operation is carried out on a smaller area increasing the chance of finding more fields and the new thresholded image will give us the proper foreground markers after some morphological operations. The results of the 1$^{st}$ and 2$^{nd}$ step of Otsu thresholding implementation on field #6 of the Ikonos satellite image are given in Figure 3.13**.**

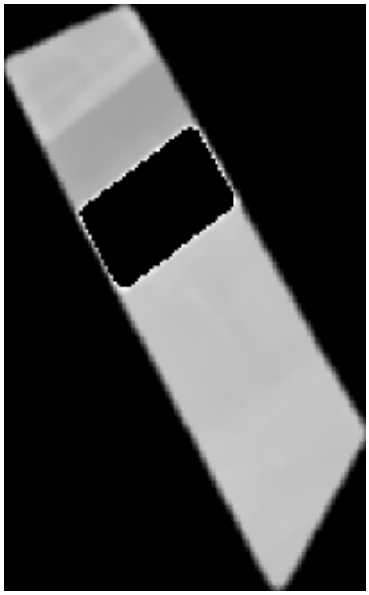

**Figure 3.12.** Masking out of the 1$^{st}$ step thresholding from the original image

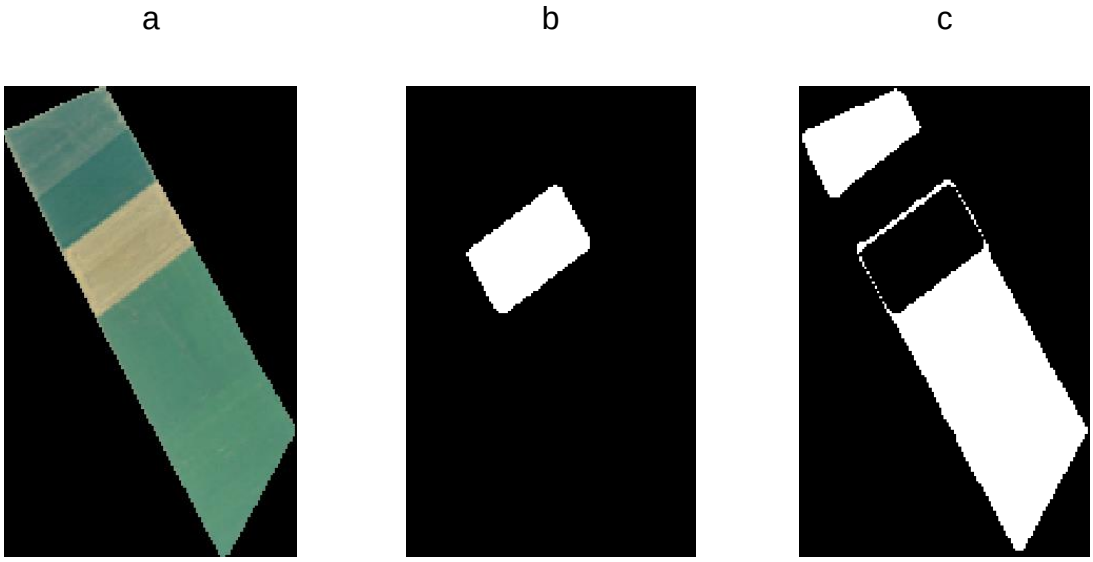


**Figure 3.13.** (a) The Ikonos image for Field #6 (b) The result of 1st step of Otsu thresholding, (c) The result of 2nd step of Otsu thresholding

### 3.2.4. Morphological Processing

The meaning of morphology is the form and design of an object or the arrangements and relation between the parts of that object. Generally morphology deals with the shape of objects. The digital form of morphology is a way of analyzing for describing the shape of a digital object (frequently raster form) [71]. The first use of morphology is related to biology, but nowadays, mathematical morphology is one of the most essential operators for digital image processing.

Morphological operators can be applied to all types of images, but the simplest form of these operators is the binary image morphology (that is used in the proposed method). Hole filling and Erosion are the operators that are used in this study.

A structuring element is a rectangular array of pixels (small binary image), that contains the value of 1 or 0 (akin to a small binary image) [72]. A few examples of structuring elements are shown here in Figure 3.14.

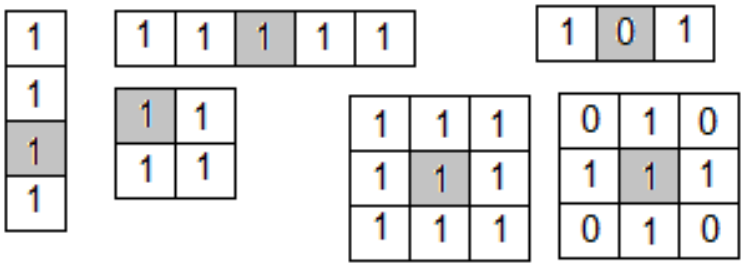


**Figure 3.14.** The structuring elements with different shapes and sizes

Structuring elements (SE's), are always designed as center pixel. One of the important issues with morphological operators, is how to choose the SE properly in order to have delicate results.

In other words, SE is nothing but a small set used to probe the image under study [73]. Figure 3.15 shows the implemented structuring element that is used in the proposed method.

**Figure 3.15.** The implemented structuring element in this study

### 3.2.4.1. Morphological Erosion

Morphological erosion is "thinning" or "shrinking" of objects in an image. The question that comes to mind, when we probe a set with a SE is: "whether the SE fits the set or not?"

The erosion of $X$ by $B$ is defined as:

$$X \ominus B = \{Z|(B)_z \cap A^c \neq \emptyset\} \quad (3\text{-}18)$$

This means, erosion of $X$ by $B$ is the set of all SE origin locations where the translated B dose not overlap with the background of $X$. $B$ is placed into each point of $X$. If $X$ AND $B$ is not equal to zero, then B is inserted in the output image [74]. So the eroded set is the location of points where the SE fits the set. Figure 3.16 shows

the process of erosion and some examples of applying erosion on a binary image are shown in Figure 3.17.

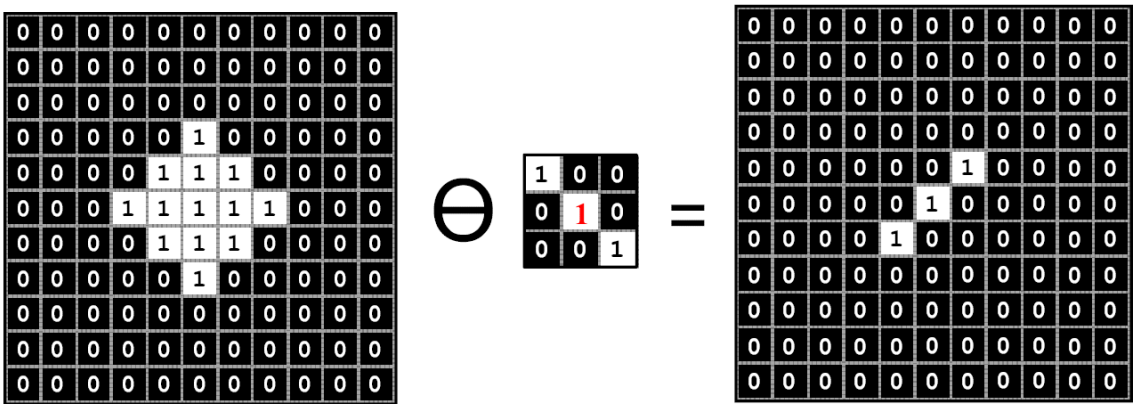

**Figure 3.16.** Illustration of erosion

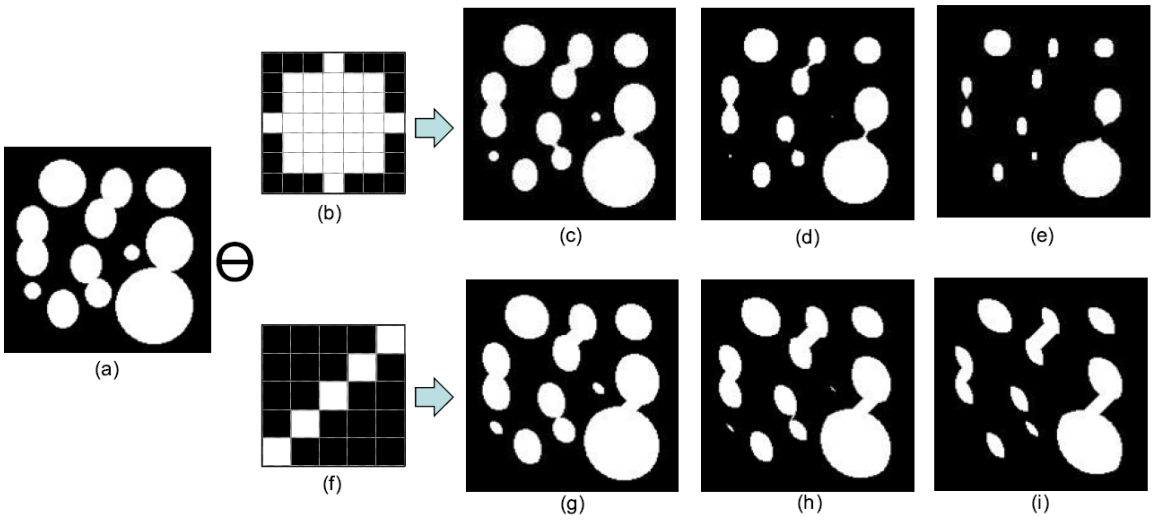


**Figure 3.17.** Implementation of two structuring elements (b & f) on the image (a). (c) After one erosion, (d) after twice and (e) after three times erosion of (a) by (b) (g) After one erosion, (h) after twice and (i) after three times erosion of (a) by (f)

### 3.2.4.2. Morphological Hole Filling

Filling the value "1" into the entire object region is the objective of hole filling [75]. An object (set "$A$") in a binary image contains boundary pixels (1) and non-boundary pixels (0). By allocating "1" to a pixel "$p$" inside the set "$A$", and then growing it by applying an iterative dilation operation under a limited circumstance, restricted by "$A^c$", the hole filling operation starts. The restriction process is for preventing the

growing process from flooding the whole image area. The iteration process that will be done in the $k$th step is defined as [69]:

$$X_k = (X_{k-1} \oplus B) \cap A^c \, , k = 1,2,3, \ldots \quad (3\text{-}19)$$

Where $B$ is the SE and $X_0 = p$ is the initial step. As shown in Figure 3.19, the iteration will be stopped at the $k$th step, if "$X_k = X_{k-1}$", so "$X_{k-1}$" is the initial region of the interested object set "$A$". The hole filling operation will be done with the union of "$X_{k-1}$" and "$A$". An example for hole filling is shown in Figure 3.18.

a b

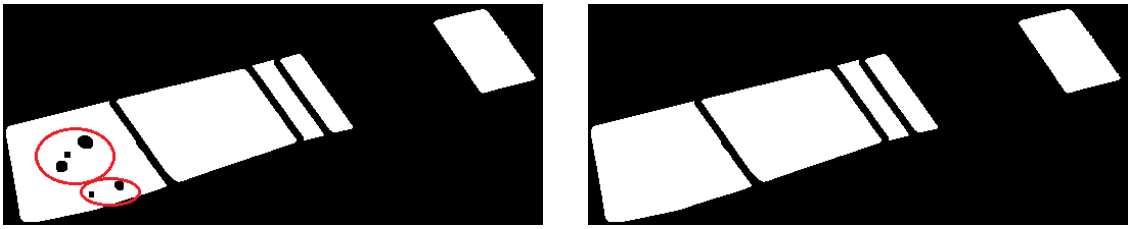

**Figure 3.18.** The implementation of hole filling on Field #4 (a) The original binary image after Otsu thresholding with the holes that are shown by red circles (b) The result of hole filling operation on (a)

### 3.2.4.3. Using Mathematical Morphology in the Proposed Method

In this part of the proposed method, erosion is the only used morphological operator. The effect of erosion on the output of section 3.3, applied on the field#6 is shown below in Figure 3.20

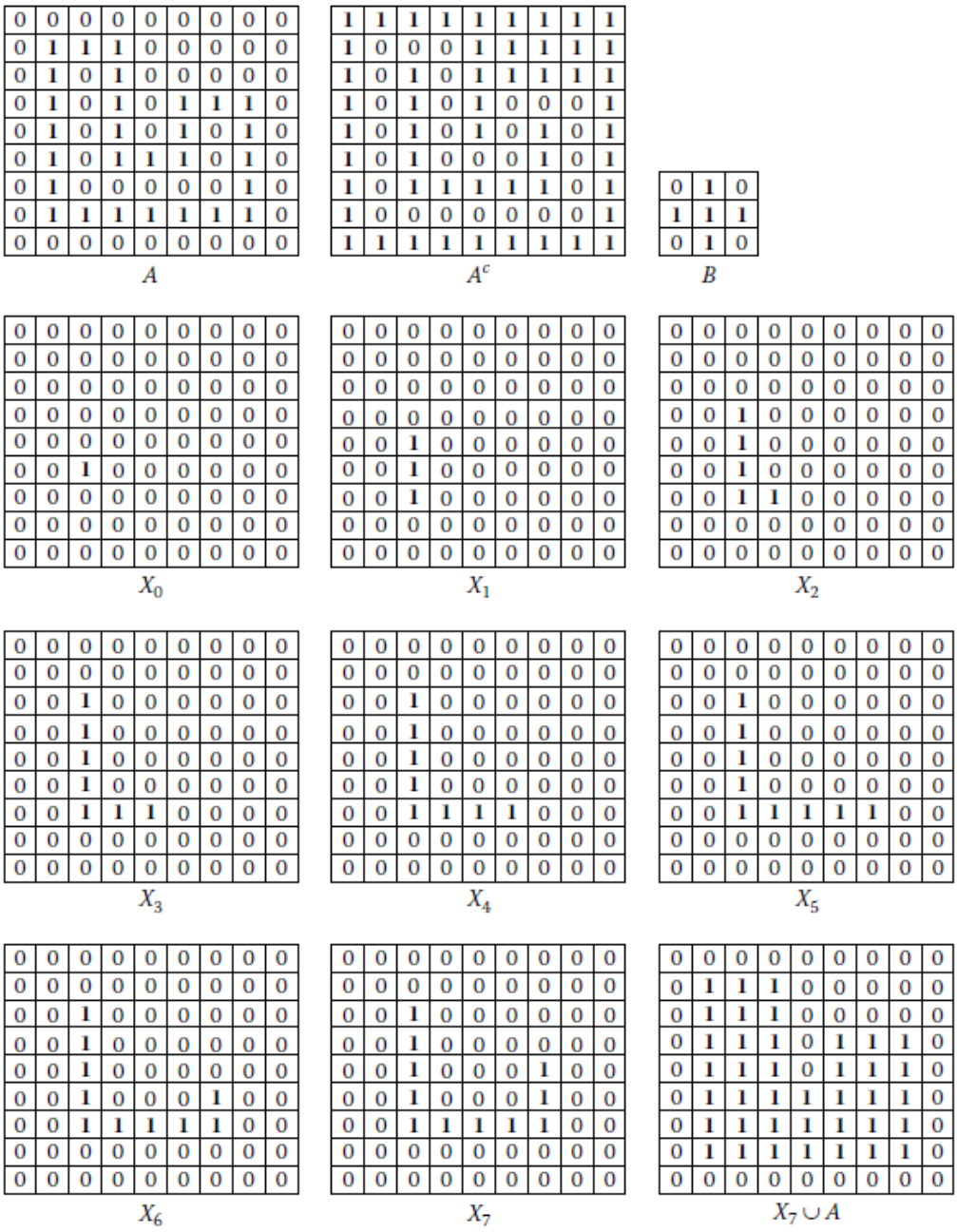


**Figure 3.19.** Hole Filling using mathematical morphology [75]

a b

**Figure 3.20.** Implementation of Erosion on Field #6 (a) Output of second step of Otsu thresholding with the additional strips that are shown with the red circle (b) implementation of Erosion operation that eliminate the additional strips

### 3.2.5. Reversing and Union Step

After applying the morphological erosion operation, the binary output image is ready for the final step through which a reversing operation is carried out to detect the areas in which the final foreground markers are to be seeded. With this respect, the values of “1” are assigned the values of “0” and the values of “0” are assigned the values of “1” in order to have proper markers in the output. As shown in Figure 3.20, the output image of this step is not a proper marker for the proposed method. Therefore, after the reversing step operation, morphological operators, hole filling and erosion, will be applied (Figure 3.21).

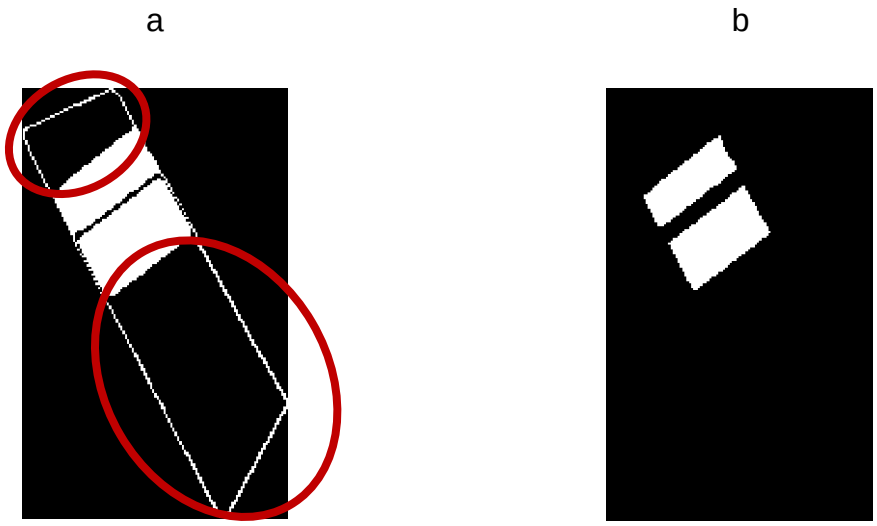


**Figure 3.21.** (a) Output of reversing step of Field #6 with the additional strips that shown with the red circle (b) implementation of Erosion operation that eliminate the additional strips

As shown in Figures 3.20 and 3.21, the 2 outputs of section “3.2.3”, the second step of Otsu thresholding, and this section complete each other. So the union of these two, gives us the proper and required marker image for following steps of planned method. Figure 3.22 shows the final foreground marker for field #6.

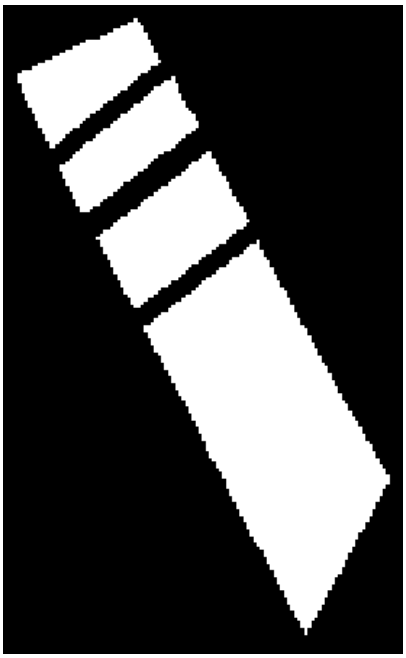

**Figure 3.22.** Final foreground markers for Field #6

### 3.3. Watershed Segmentation

In geography, a watershed is the ridge that divides the area drained by different river system. A catchment basin is the geographical area draining into a river or reservoir [69]. Applying these ideas to image processing for solving the image segmentation problems is the watershed transform.

An image should be considered as a topographic surface for explaining the watershed transform. On this surface, the pixel values of $f(x, y)$ represent the heights. Figure 3.23 explains these terms [74]. Figure 3.23.a is the explained surface and 3.23.b is the 3D representation of that surface:

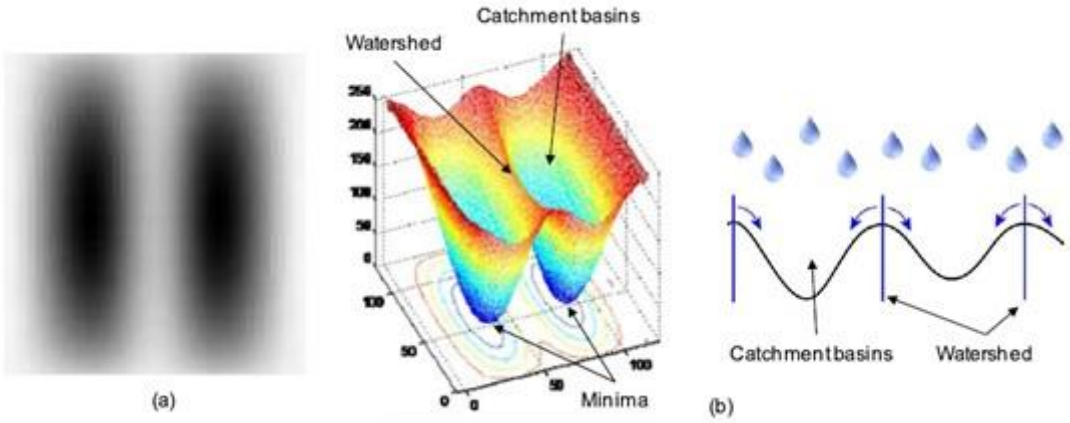


**Figure 3.23.** Watershed transform

Imagine a rain falling on this surface. It is obvious that the falling rain would accumulate in the two catchment basins. By preventing the water coming from different sides from merging, the image would be partitioned into two different sets of catchment basins and the watershed ridge lines. The watershed transform finds exactly these two portions in the image for solving the segmentation problems.

#### 3.3.1. Watershed Segmentation Using the Gradient

One of the major problems using watershed transform for image segmentation is the over segmentation [66]. Noise, variety of surface, etc. are the reasons of this over segmentation. Using the gradient of an image instead of the image itself is a good way to prevent these over segmentations. As mentioned in section 3.1.3, the gradient magnitude has high gray-level values at the edges. In an ideal situation,

the edges of the objects represent the watershed ridge lines. This means, ideally, the watershed transform would result in watershed ridge lines along the object boundaries [69]. Figure 3.24 is an illustration of this method.

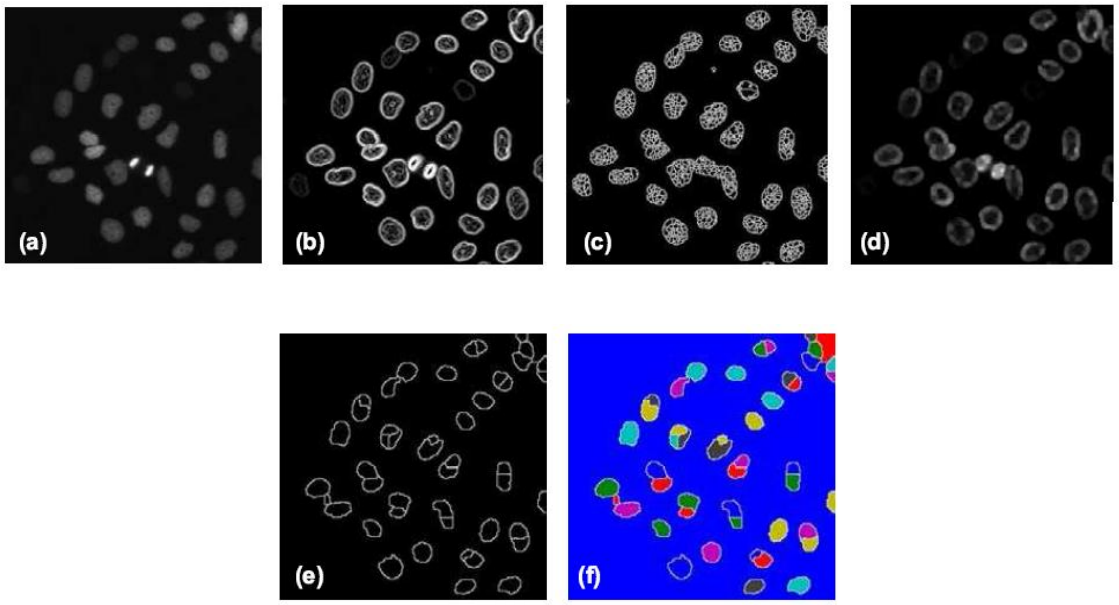


**Figure 3.24.** Watershed segmentation using the gradient. (a) A grayscale image of nuclei, (b) The gradient magnitude of (a), (c) Watershed transform of gradient image, (d) Applying a smoothing filter to gradient for overcoming the over segmentation, (e) Watershed transform of (d), and (f) is the colored representation of segmented objects

### 3.3.2. Marker Controlled Watershed Segmentation

As illustrated in the previous section, direct implementation of the watershed transform to the gradient magnitude image, causes over-segmentation problems. Markers are the concept for controlling this problem. The marker-controlled watershed segmentation is a robust and flexible method for the segmentation of objects with close boundaries, where the boundaries are expressed as ridges [67]. A marker is a united component belonging to an image [69]. There are two kinds of general markers: Foreground or internal markers that take place inside the object, and background or external markers that are contained in the background and somehow they make up the ridge lines. The foreground marker image used for the

marker-controlled method is a binary image of either single marker points or a large connected marker regions. Each marker takes its place inside only one object. The number of initial markers represent the number of objects in the segmented image. This is because of the one-to-one relation between the markers and objects in the image [67]. There are various methods for computing the markers. As explained before in section 3.2.5, a combination of special Otsu thresholding and morphological operations is used in the proposed method in this thesis. Figure 3.25 shows the implementation of marker-controlled watershed segmentation of nuclei image[74].

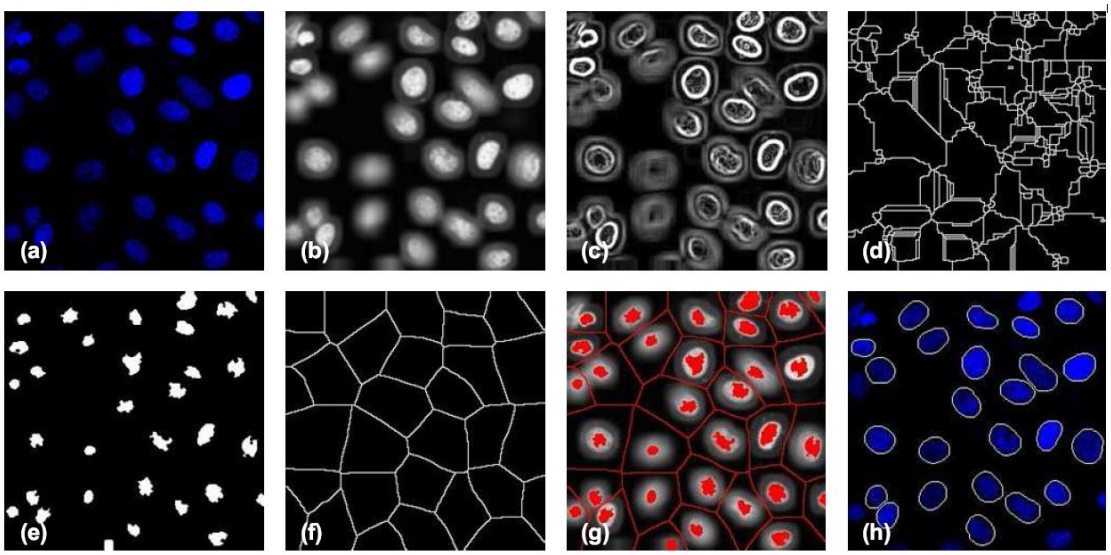


**Figure 3.25.** Marker-controlled watershed segmentation. (a) Gray scale image of nuclei, (b) Gradient magnitude, (c) Watershed transform of gradient image, (d) Watershed ridge line of gradient, after applying a smoothing filter, (e) Marker image, (f) Watershed ridge lines, (g) Imposition of gradient and markers and watershed ridge lines, (h) Result of segmentation

Because the segmentation is carried out within agricultural fields to extract within-field sub-fields and the outside fields are not of interest there is no need for the background markers therefore.

The proposed method uses the result of section 3.1.3 and 3.2.4 for completing the marker controlled watershed segmentation task. This task is carried out by imposing the markers to the gradient magnitude and segmenting this image using Matlab software watershed segmentation algorithm.

### 3.4. Accuracy Assessment

The results were assessed by comparing the geometry of automatically detected outputs with the manually defined segments that are used as the reference data. The reference segments were defined manually using the Adobe Photoshop CS6 software. The assessment approach is primarily based on finding the differences between the positional and interpretation errors easily [76]. The concept is based on the overlaying of automatically extracted objects and manually segmented object geometries.

The match between the two objects ("$M_{ij}$") can be indicated as a geometrical mean of the two conditional probabilities of "$M_i$" and "$M_j$" as shown below:

$$M_{ij} = \sqrt{M_i . M_j} \tag{3-20}$$

$$M_i = {Area(i \cap j)}\Big/{Area(i)} \tag{3-21}$$

$$M_j = {Area(i \cap j)}\Big/{Area(j)} \tag{3-22}$$

Where "$M_{ij}$" gets a value between "1" and "0". If two sets have no matching, the "$M_{ij}$" will have the value "0" and the value "1" for "$M_{ij}$" shows that 2 sets are completely matched.

The matching percentage value between the reference data and automatically detected results, which were extracted using proposed approach, are computed to assess the accuracy of the results. This task will be done by constructing a $m \times n$ matrix which contains the matching values between reference fields and segments. This $m \times n$ size of the matrix is due to the difference between the number of fields in the reference data and the segmentation results.

For better understanding the concept, the calculation of matching values for a sample field is illustrated below in Figure 3.26 [16].

Reference Segment

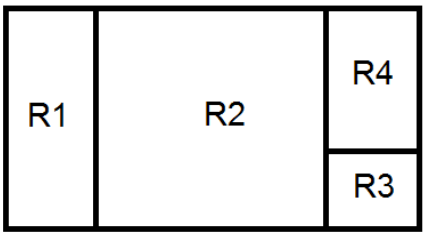


Area (R1) = 4

Area (R2) = 6

Area (R3) = 1.5

Area (R4) = 2.5

Calculated Segment

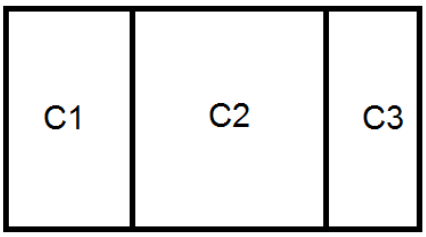


Area (C1) = 5

Area (C2) = 5

Area (C3) = 4

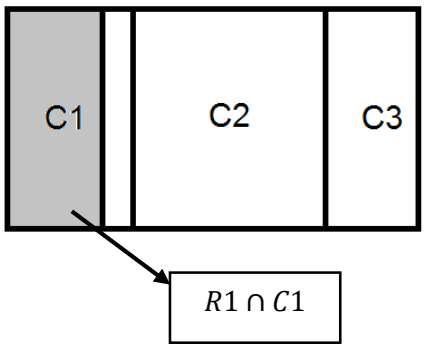


$M_{1,1} = 0.89$

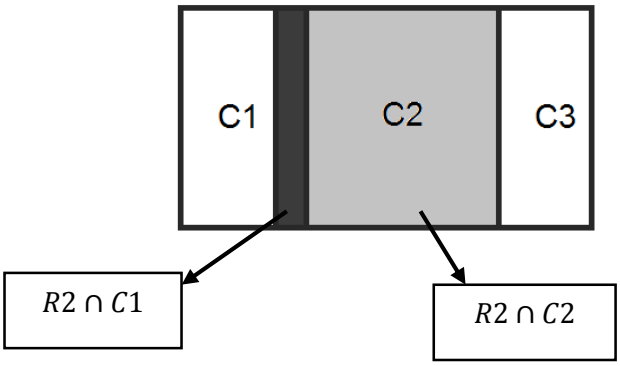


$M_{2,1} = 0.18$ $M_{2,2} = 0.91$

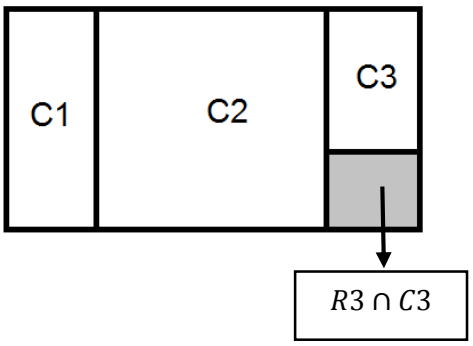


$M_{3,3} = 0.61$

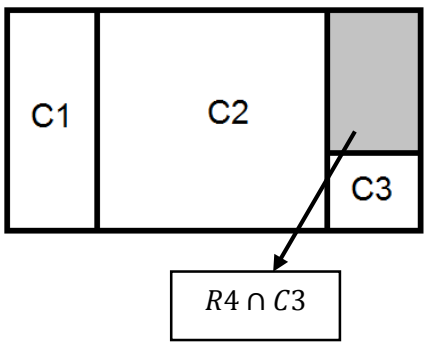


$M_{4,3} = 0.79$

$$M = \begin{array}{c} \\ R1 \\ R2 \\ R3 \\ R4 \end{array} \begin{array}{c} \begin{array}{ccc} C1 & C2 & C3 \end{array} \\ \begin{bmatrix} 0.89 & 0 & 0 \\ 0.18 & 0.91 & 0 \\ 0 & 0 & 0.61 \\ 0 & 0 & 0.79 \end{bmatrix} \end{array}$$

**Figure 3.26.** Comparison of geometries between reference fields and calculated fields for sample field

R1, R2, R3 and R4 stand for reference segments and C1, C2 and C3 stand for the calculated segments. The matching value between R1 and C1 is computed as 0.89 and assigned to "$M_{1,1}$". "$M_{1,2}$" and "$M_{1,3}$" become zero, because, there is no overlap between R1 and C2, C3. The matching value of other fields, R2, R3 and R4 are computed as below:

$$R2 \cap C1 = 0.18 \qquad R2 \cap C2 = 0.91 \qquad R2 \cap C3 = 0$$

$$R3 \cap C1 = 0 \qquad R3 \cap C2 = 0 \qquad R3 \cap C3 = 0.61$$

$$R4 \cap C1 = 0 \qquad R4 \cap C2 = 0 \qquad R4 \cap C3 = 0.79$$

As it can be seen in Figure 3.26, C1 and C2 have multiple matching values. In this case, specific threshold can solve this problem. In this approach the threshold value is defined as "0.75" that is represented by [77] for the evaluation of the segmentation outputs. Therefore, the multiple values would be deleted from the matrix. For analyzing the matching percentage values for the fields, the mean value is computed by dividing the sum of the values by the number of reference segments. Following this concept, the mean of the matching value in Figure 3.26 is calculated as:

(0.89+0.91+0+0.79)/4=0.648

So, the overall accuracy percentage of the example field, would be 64.8%.

# 4. RESULTS AND DISCUSSIONS

## 4.1. Study Area

The study area is located in the south-west Karacabey, a town of Bursa which is situated in Marmara region in the north-west of Turkey. The size of the study area is nearly 4.6 km by 7.2 km. Because of superior weather conditions, agriculture is the basic land use in this region. The project of land consolidation of this area was accomplished between 1988 and 1992.The main agricultural use of these fields is the farming of crops and several fields are used for the grazing of the animals. Rice, sugar beet, corn, pepper, and tomatoes are the main crops which are grown in the region. 40°08’48’’ to 40°12’42.4’’N and 28°14’14.2’ to 28°17’31’’E are the coordinates of the study area in UTM zone 35.

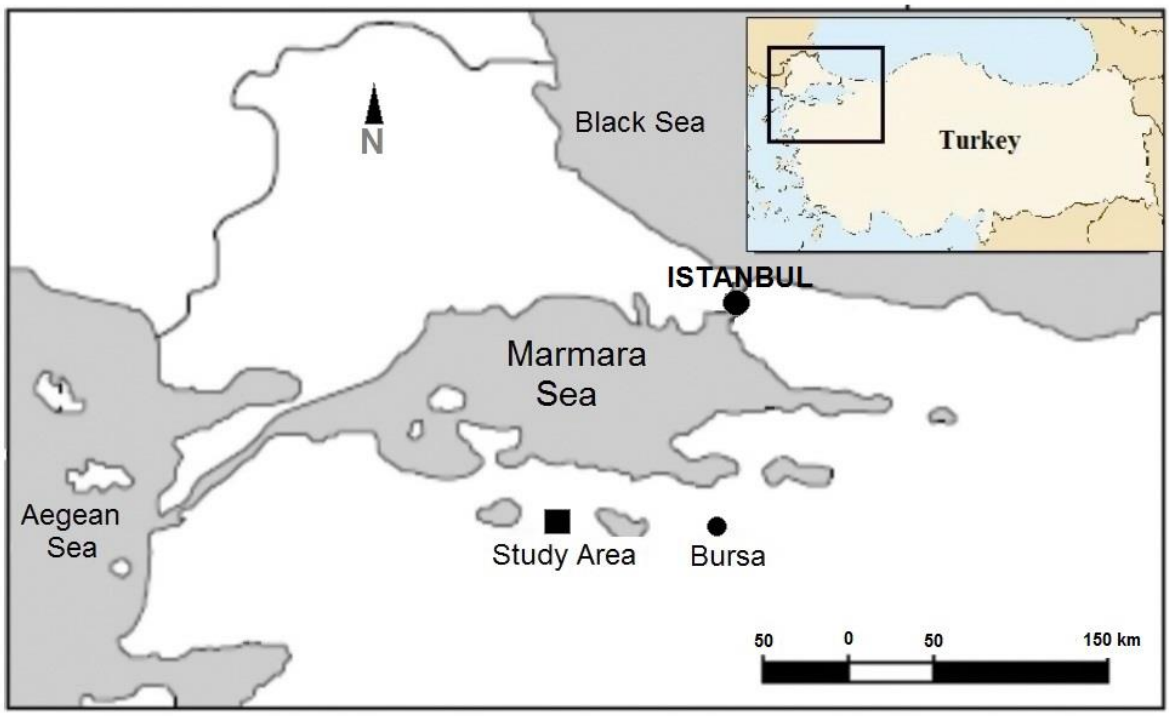


**Figure 4.1.** The location of study area in Turkey

## 4.2. Data Sets

According to the nature of the proposed segmentation method, which is based on the integration of image data and field boundary information, the segmentation operation needs two types of datasets as input datasets, which are satellite imagery data and agricultural field boundary data.

### 4.2.1. Satellite Imagery Data

The satellite imagery data, which were used in this study and their acquisition dates are shown in Table 1. Further, the satellites' characteristics are shown in Table 2.

**Table 1.** Used raster data

| Dataset | Acquisition Date |
|---|---|
| Ikonos Multispectral (XS) | 15.07.2004 |
| QuickBird XS | 13.08.2004 |
| QuickBird Pan sharpened (PS) | 13.08.2004 |
| Spot 5 | 22.07.2004 |

**Table 2.** The spectral and spatial specifications of the satellite data used

| Satellite | Spectral Bands | Spectral Range (nm) | Spatial Resolution (m) |
|---|---|---|---|
| Ikonos | Panchromatic | 445 – 900 | 1 |
| | B1: Blue | 450 – 520 | 4 |
| | B2: Green | 520 – 600 | 4 |
| | B3: Red | 630 – 690 | 4 |
| | B4: Near IR | 760 – 900 | 4 |
| QuickBird | Panchromatic | 450 – 900 | 0.65 |
| | B1: Blue | 450 – 520 | 2.62 |
| | B2: Green | 520 – 600 | 2.62 |
| | B3: Red | 630 – 690 | 2.62 |
| | B4: Near IR | 460 – 900 | 2.62 |
| Spot 5 | Panchromatic | 480 – 710 | 5 |
| | B1: Green | 500 – 590 | 10 |
| | B2: Red | 610 – 680 | 10 |
| | B3: Near IR | 780 – 890 | 10 |
| | B4: Shortwave IR | 1580 – 1750 | 20 |

### 4.2.2. Field Boundary Data

The permanent field boundaries which are available in the digital vector form, were digitized from the cadastral map sheets in a previous study conducted by [78]. Therefore, the agricultural field boundaries were already available. The boundaries were in UTM projection system. A formatted text file which includes the perimeter, area, identification numbers and some other properties were stored in a GIS database. In this thesis, the existing permanent field boundaries were used as reference data to assess the segmentation results.

## 4.3. The Results of Intensity Image

In this thesis, four different spatial resolution images were used (Table 1). As mentioned in Section 3.1.1(RGB to Intensity transformation), the experimental tests were carried out on the Intensity images that are calculated from the original bands, R, G and B, of the Ikonos and QuickBird images, and R, G and NIR bands, of the Spot5 images (because there is no Blue band in Spot5).

The empirical tests of the proposed method were carried out on the selected 20 agricultural fields which were randomly chosen in various shapes and sizes for testing the abilities of the method. The size of the fields range from 5.92 ha (field #14) to 77.37 ha (field #4), and the number of subfields the fields contain range from 2 to 13. However, the number of subfields the fields contain may differ on each image due to the acquisition date of the imagery. For example, as it can be seen in Table 4, field #4 contains 7 subfields in the Ikonos XS and QuickBird PS images, whereas this field contains 8 and 5 subfields in the QuickBird XS and Spot5 XS images, respectively. For the test fields the areas calculated are given in Table 3.

The number of subfields for each imagery used and the number of subfields which were detected through the developed segmentation method, are shown respectively in Tables 4 and 5.

**Table 3.** The sizes of the test fields

| Field ID | Area (ha) | Field ID | Area (ha) | Field ID | Area (ha) | Field ID | Area (ha) |
|---|---|---|---|---|---|---|---|
| **1** | 22.95 | **6** | 14.05 | **11** | 29.51 | **16** | 21.39 |
| **2** | 22.73 | **7** | 29.48 | **12** | 22.24 | **17** | 20.33 |
| **3** | 29.73 | **8** | 21.47 | **13** | 26.87 | **18** | 9.31 |
| **4** | 77.37 | **9** | 10.44 | **14** | 5.92 | **19** | 16.37 |
| **5** | 20.41 | **10** | 27.80 | **15** | 16.19 | **20** | 29.46 |

**Table 4.** The number of subfields in each field

| Field ID | The Number of Sub-Fields | | | |
|---|---|---|---|---|
| | Ikonos XS | QuickBird XS | QuickBird PAN | Spot XS |
| **1** | 11 | 11 | 12 | 10 |
| **2** | 10 | 10 | 10 | 8 |
| **3** | 7 | 8 | 7 | 5 |
| **4** | 6 | 7 | 7 | 7 |
| **5** | 2 | 2 | 2 | 2 |
| **6** | 4 | 3 | 3 | 4 |
| **7** | 6 | 5 | 6 | 6 |
| **8** | 3 | 3 | 3 | 3 |
| **9** | 7 | 7 | 7 | 4 |
| **10** | 4 | 4 | 4 | 5 |
| **11** | 2 | 3 | 4 | 2 |
| **12** | 4 | 3 | 3 | 3 |
| **13** | 4 | 3 | 3 | 4 |
| **14** | 4 | 4 | 4 | 4 |
| **15** | 7 | 9 | 6 | 6 |
| **16** | 11 | 9 | 9 | 10 |
| **17** | 4 | 3 | 3 | 2 |
| **18** | 6 | 7 | 7 | 6 |
| **19** | 3 | 2 | 3 | 3 |
| **20** | 13 | 13 | 11 | 11 |

**Table 5.** The number of subfields which were detected through the proposed segmented method

| Field ID | The Number of Detected Sub-Fields | | | |
|---|---|---|---|---|
| | Ikonos XS | QuickBird XS | QuickBird PAN | Spot XS |
| **1** | 12 | 9 | 6 | 8 |
| **2** | 9 | 9 | 9 | 7 |
| **3** | 8 | 6 | 5 | 5 |
| **4** | 6 | 6 | 6 | 6 |
| **5** | 2 | 2 | 2 | 2 |
| **6** | 4 | 3 | 5 | 3 |
| **7** | 6 | 9 | 7 | 6 |
| **8** | 3 | 3 | 3 | 3 |
| **9** | 7 | 7 | 6 | 4 |
| **10** | 5 | 5 | 4 | 3 |
| **11** | 2 | 6 | 6 | 2 |
| **12** | 6 | 7 | 5 | 4 |
| **13** | 4 | 8 | 6 | 4 |
| **14** | 4 | 5 | 4 | 6 |
| **15** | 6 | 8 | 5 | 5 |
| **16** | 8 | 9 | 9 | 8 |
| **17** | 4 | 4 | 4 | 3 |
| **18** | 4 | 5 | 7 | 4 |
| **19** | 3 | 2 | 4 | 3 |
| **20** | 15 | 14 | 10 | 9 |

During the implementation of the proposed method, two filter sizes were needed to be defined (mean and median filter). These filter sizes are adaptable and the user can change them as desired. For each image used, these filter sizes, were defined experimentally. The filter sizes which were used in this study are given in Table 6.

**Table 6.** The filter sizes used for each imagery system

| The parameters/ value | Ikonos XS | QuickBird XS | QuickBird Ps | Spot5 XS |
|---|---|---|---|---|
| Mean filter size | 3×3 | 3×3 | 3×3 | 3×3 |
| Median filter size | 3×3 | 11×11 | 27×27 | 3×3 |

The overall accuracies of the detected subfields by the proposed automatic segmentation method, are shown in Table 7. As it can be seen in Table 7, the Ikonos XS images provided the highest overall accuracy of 89.72%. For the QuickBird XS, QuickBird PS and Spot5 XS image, the overall accuracies were computed as 83.24%, 78.88% and 80.34%, respectively. The main reason for Ikonos imagery to give higher accuracy value is that it has lower within-field variation than the QuickBird XS and QuickBird PS images. Also have higher between-field variation than the spot5 XS. The reasons for these accuracy differences will be explained by more details, later in the following sections (4.3.1, 4.3.2, 4.3.3, 4.3.4 and 4.3.5) of this chapter.

**Table 7.** The overall accuracies computed for each group of images

| Data Set | Overall Accuracy |
|---|---|
| Spot5 XS | 80.34 |
| Ikonos XS | 89.72 |
| QuickBird XS | 83.24 |
| QuickBird PS | 78.88 |

For each image, the grouping of the segments detected through the proposed approach based on equal segmentation, over segmentation and under segmentation are given in Table 8. Equal segmentation means that the number of subfields that the proposed method detected are equal to the reference segments. Over-segmentation means that the number of detected segments are more than the reference segments, while under-segmentation means that the number of detected segments are less than the reference segments. As it can be seen in the Table 8, the proposed algorithm has the most accurate result about finding the equal segmentation in the Ikonos XS and Spot5 XS images. However, the Ikonos has more balanced results about the over and under segmentation than the Spot5. As can be seen, the number of over and under segmentations is almost equal in the Ikonos images (4 and 5) but it has vastly different results in the Spot5 images. The Spot5 images have just one over segmented result and eight under segmented

results. In the case of QuickBird images, both XS and PS, the results are pretty close.

**Table 8.** The grouping of results by the number of segments

| Data Set | | Ikonos XS | QuickBird XS | QuickBird PS | Spot5 XS |
|---|---|---|---|---|---|
| Segmentation Grouping | Equal Segmentation | 11 | 6 | 7 | 11 |
| | Over Segmentation | 5 | 8 | 7 | 1 |
| | Under Segmentation | 4 | 6 | 6 | 8 |
| Total | | 20 | 20 | 20 | 20 |

### 4.3.1. The Results of Ikonos Multispectral (XS) Images

The segmentation results of the Ikonos XS imagery and the reference data are given in Table 9. The grouping of the test fields based on their accuracy values are provided in Table 10. As it can be seen in Table 10, 15 fields have accuracies above 85%. Holistically observing, the table shows that 75% of the results are above the ideal value which means that the proposed method has worked perfectly in this group. Field #5 with an accuracy value of 99.11% has the best result within this group (85-100% accuracy value), as well as in the Ikonos XS image category. This field contains just two sub-fields and the high difference of brightness value between the two sub-fields and no within-field variation are the reasons of the high accuracy of this field. Felds #4, #6, #7, #8, #9, #10, #11, #13 and #19 also have accuracy values above 95% because of high intensity value variation between the adjacent subfields. Indeed, these results show the reliability of the proposed segmentation method. Fields #3, #12 and #14 have accuracies above 90%. These fields have some within-field variation that leads to having small false segments, but because of the small size of these segments, they do not affect the accuracy value so much.

As it can be seen in Table 10, three fields (#16, #17 and #20) have accuracy values between 70 – 84%. In field #17, the method found all the 4 segments, but because

of the little size of one of the segments, the intersection of this segment with the reference data is less than 75% [16], therefore the accuracy value falls down accordingly.

The lowest accuracy values belong to fields #15 and #18, with the accuracy values between 50 – 69%, but still above 60%. Of these fields, field #18 has the lowest accuracy value of 63.81%. After checking the result, it was observed that there was just one missing field in the result segmented image. However, because of the low overlap of the segmented sub-field with the reference data, the accuracy value has fall significantly. Yet, one missed subfield show the trustworthiness of the proposed method.

Field #15 is one of the challenging fields in this category. This field has 3 sub-fields perpendicular to a field which itself has interference with them. Checking the result shows that the challenging fields were segmented as well as the reference data. However, the existence of a missing subfield was inevitable and therefore caused the accuracy to fall. On the other hand, finding 6 subfields out of 7, shows the perfectness of the developed method. The fields #5, #7, #11, #12, #13 are indeed challenging fields that illustrate the performance of the proposed method. In these fields, one side of the field is longer than the other side of the image. The high accuracy of the results of these fields demonstrates the supremacy of the method. Fields #1 and #19 are the good cases because of the existence of intersection. The high accuracy and segmenting the intersecting subfields are the other reasons for proving the perfectness of the developed method.

**Table 9.** The results of Ikonos XS images

| # | Original Field | Reference Segments | Result Segments | Accuracy (%) |
|---|---|---|---|---|
| **1** | | 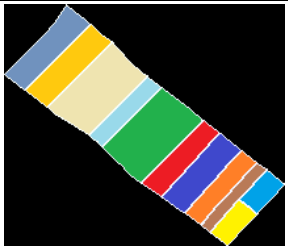 | 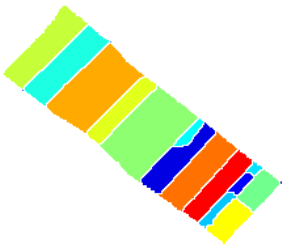 | 87.55 |

| | | | | |
|---|---|---|---|---|
| **2** | 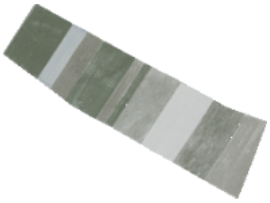 | 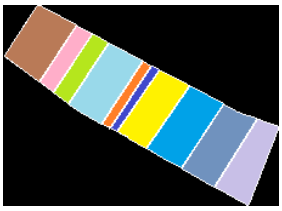 | 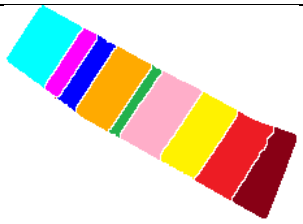 | 86.61 |
| **3** | | 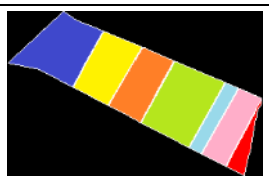 | 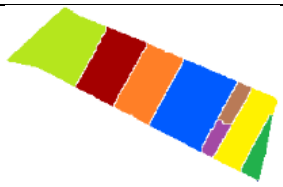 | 94.21 |
| **4** | | 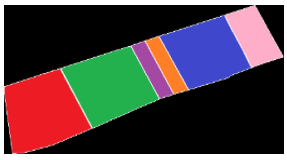 | 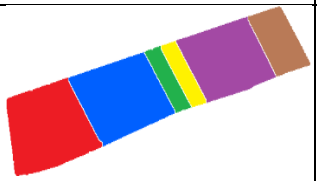 | 98.71 |
| **5** | | 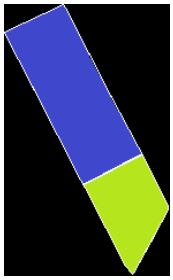 | 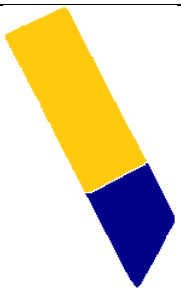 | 99.11 |
| **6** | | 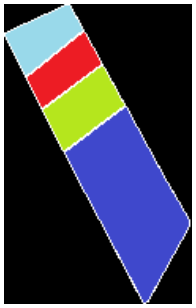 | | 98.08 |
| **7** | | 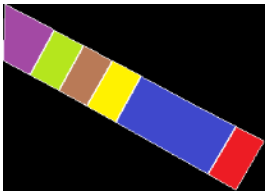 | 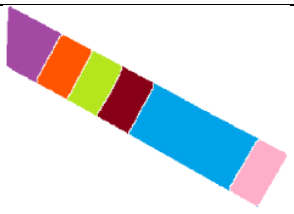 | 98.46 |
| **8** | 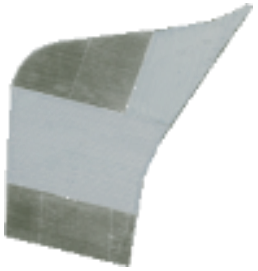 | | | 98.38 |

| | | | | |
|---|---|---|---|---|
| **9** | 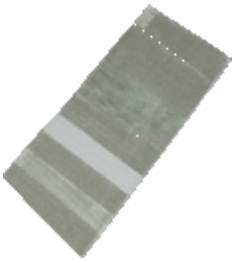 | | | 96.05 |
| **10** | | | | 97.10 |
| **11** | | 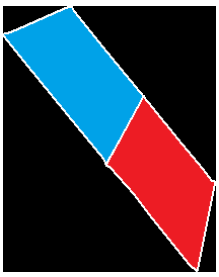 | 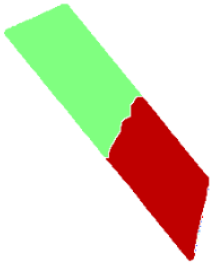 | 98.07 |
| **12** | 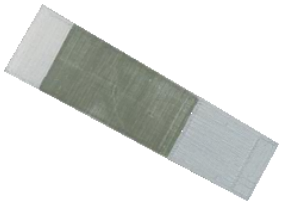 | 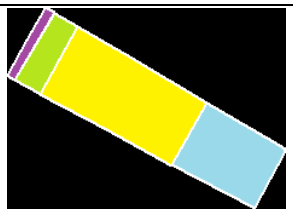 | 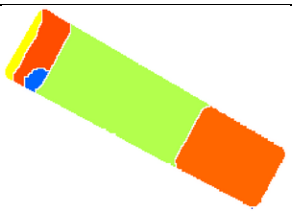 | 93.54 |
| **13** | 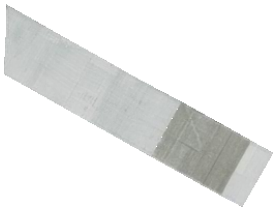 | 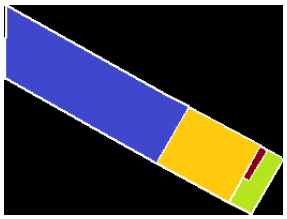 | 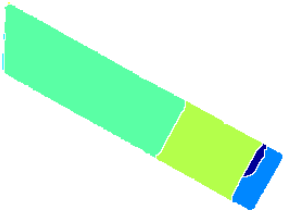 | 95.03 |
| **14** | 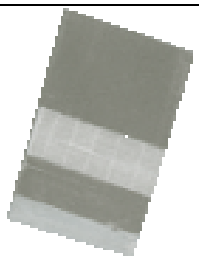 | | | 93.61 |

| | | | | |
|---|---|---|---|---|
| **15** | 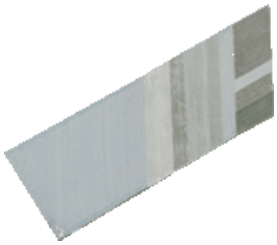 | 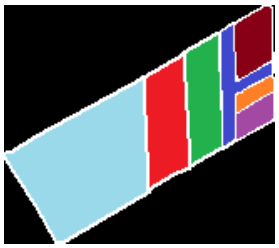 | 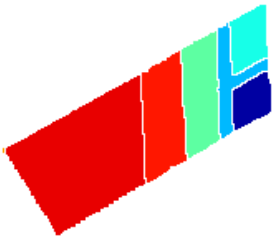 | 69.04 |
| **16** | | 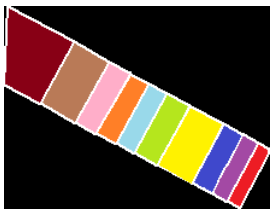 | 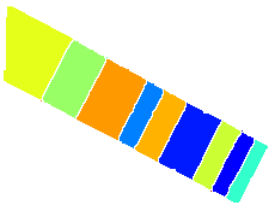 | 77.00 |
| **17** | | | | 72.63 |
| **18** | | 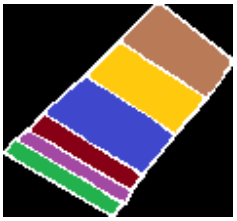 | | 63.81 |
| **19** | 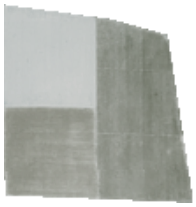 | | | 97.44 |
| **20** | | 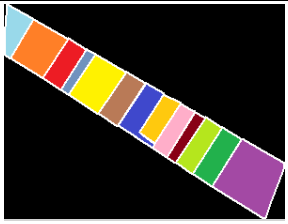 | 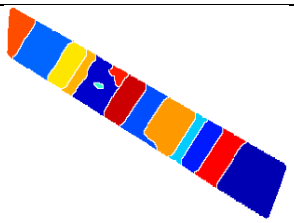 | 80.05 |

**Table 10.** For Ikonos XS imagery the grouping of the test fields based on their accuracy values

| Accuracy (%) | Fields | Total | Percentage |
|---|---|---|---|
| 85 – 100 | #1,#2,#3,#4,#5,#6,#7,#8,#9,#10,#11,#12, #13,#14,#19 | 15 | 75% |
| 70 – 84 | #16,#17,#20 | 3 | 15% |
| 50 – 69 | #15,#18 | 2 | 10% |
| 0 – 49 | - | 0 | 0% |
| Total | | 20 | 100% |

### 4.3.2. The Results of QuickBird Multispectral (XS) Images

The results of the QuickBird XS imagery and the reference data are given in Table 11. The grouping of the test fields based on their accuracy values are provided in Table 12. As it can be seen in Table 12, twelve fields have accuracies above 85%. Looking at the table, it can be seen that 60% of the results are above the ideal value and this means that the proposed method has worked perfectly in this group. Similar to previous section (Ikonos XS results) field #5 with the accuracy value 99.68% has the best result within this group (85-100% accuracy value), and also has the best result in the QuickBird XS image category. As mentioned in the last section (4.3.1), this field contains just two sub-fields and the high difference of brightness value between the two sub-fields and no within-field variation are the reasons for the high accuracy of this field. Fields #6, #7, #8, #10, #16, #17, #18 and #19 have the accuracy values above 90%. This shows that 50% of the results in this section are above the ideal value illustrating the perfectness of the proposed method.

Although fields #11, #12 and #13 have some incorrect and over segments, they all have accuracy value above 85%. The little extra segments detected within these fields are due to within-field variations that the low-pass filtering (mean and median) performed before segmentation could not remove. Because of spatial resolution of the QuickBird XS imagery (2.44m) and the existence of high details in this image, over segmentation can be considered normal. The strong within-field variation will affect the Otsu thresholding results, therefore there will be extra foreground markers

and this will lead to an over segmented result. These variations can be seen in fields #2, #7, #9, #11, #12, #13, #14, #16 and #17, but this variation has the most effect on the fields #2 and #14. The effect of this over segmentation leads to group fields #2 and #14 in the 3rd row of Table 12, because their accuracy is in the range of 50 – 69 %. Also in field #2, there are missed segments too. The low variation of the intensity image between the adjacent subfields is the major reason for the missed segments. Because the Otsu's method cannot distinguish these fields from each other, it reduces the accuracy of the results. This is the main reason of the low accuracy values computed for fields #1 and #3 too. These fields have the lowest accuracy values in Table 11 and are grouped in the last row of Table 12. These fields have the accuracy values under 50% and they illustrate the worst results of the test fields assessed using the QuickBird XS image. This is because both fields have 4 missed fields.

The accuracy value of 71.34% computed for field #15 is not a bad result for the extreme case of this field which was mentioned in the previous section. Also, for the QuickBird XS image, the proposed method has shown its great ability in case of fields #5, #7, #11, #12 and #13 (that have subfields with one side longer than other side) again. Finally, it is necessary to remind that the QuickBird XS images are very high resolution images and the overall accuracy of 83.24% shows how perfectly the proposed method is working.

**Table 11.** The results of QuickBird XS images

| # | Original Field | Reference Segments | Result Segments | Accuracy (%) |
|---|---|---|---|---|
| **1** | 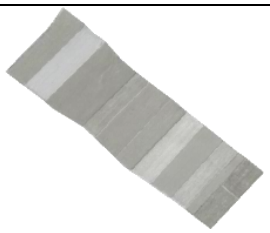 | 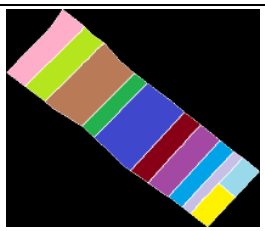 | 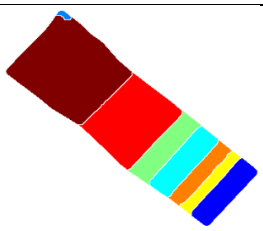 | 43.60 |
| **2** | 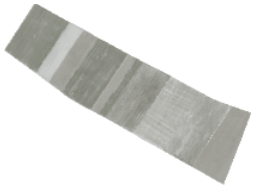 | 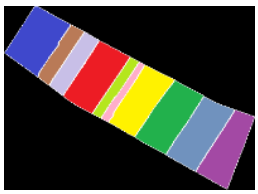 | 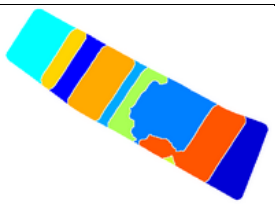 | 67.30 |

| | | | | |
|---|---|---|---|---|
| **3** | | 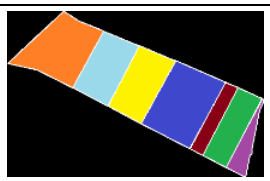 | 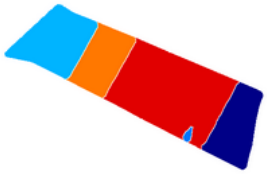 | 39.90 |
| **4** | | 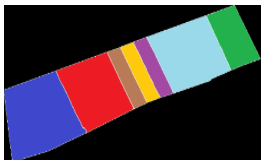 | 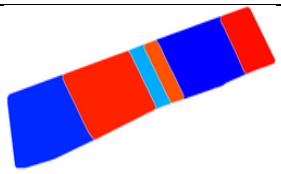 | 83.52 |
| **5** | | 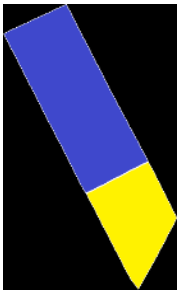 | | 99.68 |
| **6** | | 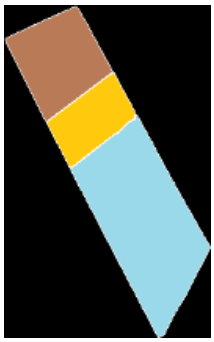 | | 98.80 |
| **7** | | 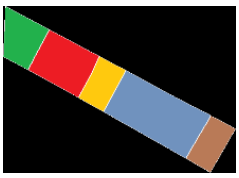 | 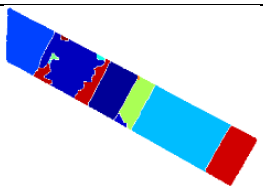 | 94.12 |
| **8** | | 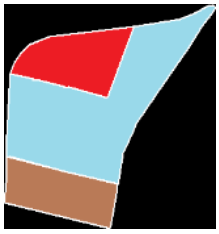 | | 98.80 |
| **9** | | 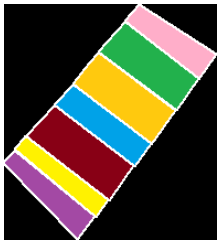 | 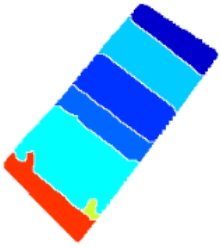 | 79.47 |

| | | | | |
|---|---|---|---|---|
| **10** | | 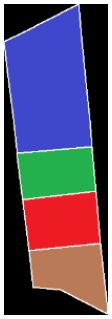 | | 96.65 |
| **11** | | 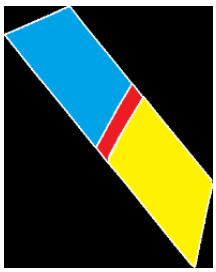 | 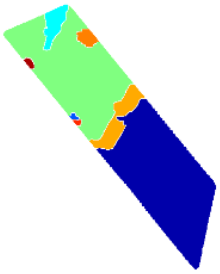 | 88.29 |
| **12** | 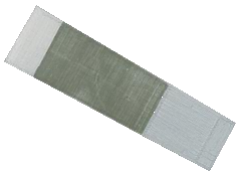 | 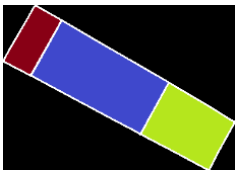 | 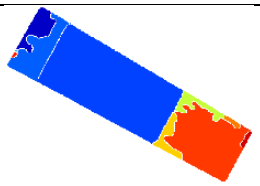 | 87.40 |
| **13** | 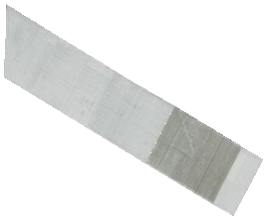 | 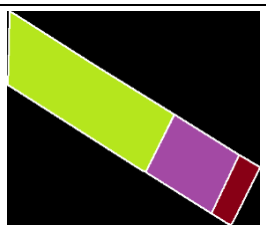 | 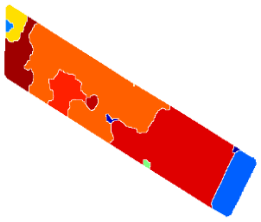 | 86.23 |
| **14** | 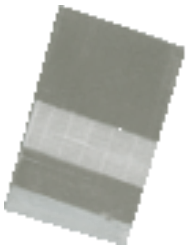 | | 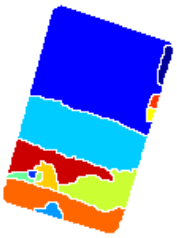 | 68.78 |
| **15** | 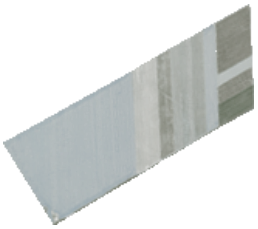 | 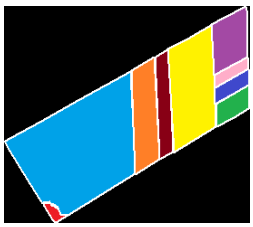 | 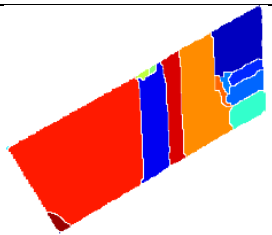 | 71.34 |

| | | | | |
|---|---|---|---|---|
| **16** | 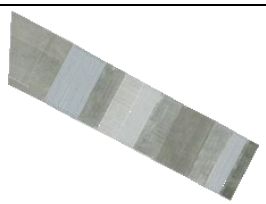 | 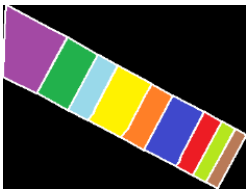 | 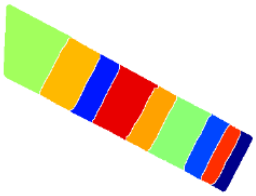 | 95.72 |
| **17** | | | | 95.13 |
| **18** | | 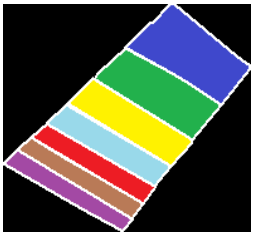 | 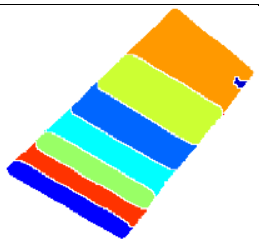 | 95.43 |
| **19** | 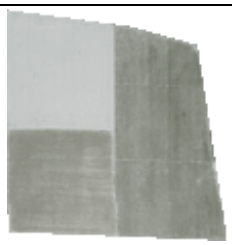 | | 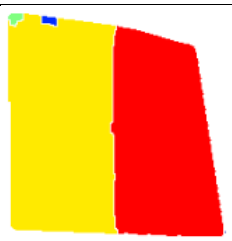 | 98.47 |
| **20** | 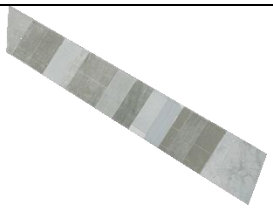 | 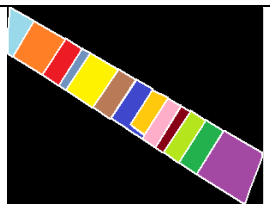 | 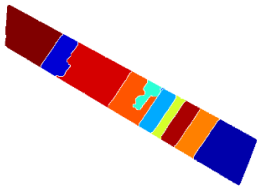 | 76.23 |

**Table 12.** For QuickBird XS image the grouping of test fields based on their accuracy values

| Accuracy (%) | Fields | Total | Percentage |
|---|---|---|---|
| 85 – 100 | #5,#6,#7,#8,#10,#11,#12,#13,#16, #17,#18,#19 | 12 | 60% |
| 70 – 84 | #4,#9,#15,#20 | 4 | 20% |
| 50 – 69 | #2,#14 | 2 | 10% |
| 0 – 49 | #1,#3 | 2 | 10% |
| Total | | 20 | 100% |

### 4.3.3. The Results of QuickBird Pan Sharpened (PS) Images

The results of the QuickBird PS imagery and the reference data are given in Table 13. The grouping of the test fields based on their accuracy values are provided in Table 14. In this section, as pointed in Table 14, 45% of the results have stayed above the ideal accuracy value of 85%. It is true to say that these results are not as good as the results provided in the two previous sections However, it is necessary to remind that the QuickBird PS image contains pixels with very high resolution, and given this condition, these results would not reduce the power of the proposed method, but increase it. Because of the small pixel size of this test image (0.61 m), it is natural to have lots of within-field variations in the test fields, and thus this would directly affect the results.

Ten fields are subject to within-field variations in this section. But this variation can't affect the results of all of these fields. Fields #11, #12, #14, #17 and #20 have the accuracy values above 80% and this is another proof for the reliability of the proposed method. Fields #2, #6, #16 and #19 have the accuracy values above 50% and it can be said that they are acceptable. But field #13 is the main victim of the within-field variation with 35.23% accuracy value and also has the worst result among the all 20 fields of this section.

Field #1 is the other bad result of this section with the computed accuracy value of 39.88%. In this case, the missed sub-fields are the reason for this low accuracy value. By looking at the intensity image of this field in Table 13, it can be seen that the missing fields do not have so much difference in their reflection values. Therefore, this reason leads to the bad result of Otsu's method and thus the missed markers.

Similar to previous two sections (4.3.1 and 4.3.2), field #5 provided the best result with the accuracy value of 99.69% in this section too.

The high resolution of this test image leads to another problem in this section and it is the strong variation in boundaries. The variation in the edges and boundaries between sub-fields is so high that it cannot be eliminated by the filtering operation and therefore it makes way to have incorrect and extra segments at the boundaries in the fields #1, #6, #7, #8, #9, #11, #14, #15 and #19.

Investigating the challenging cases, fields #5, #7, #11, #12 and 13, it can be seen that except field #13, the algorithm is very successful at the others.

**Table 13.** The results of QuickBird PS images

| # | Original Field | Reference Segments | Result Segments | Accuracy (%) |
|---|---|---|---|---|
| **1** | | 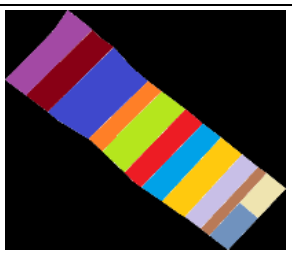 | 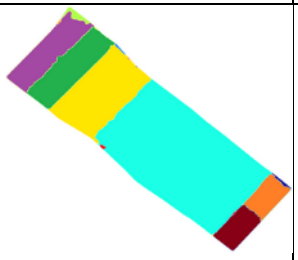 | 39.88 |
| **2** | 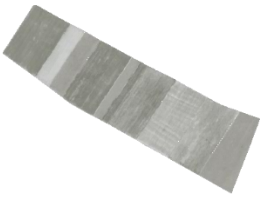 | 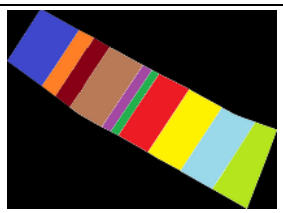 | 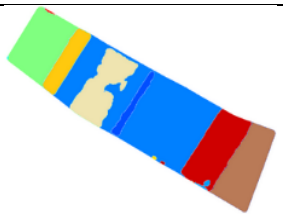 | 56.78 |
| **3** | | 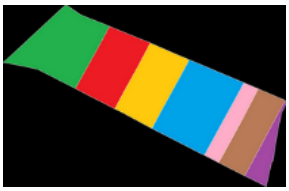 | 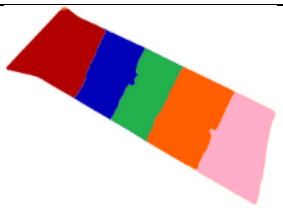 | 55.93 |
| **4** | | 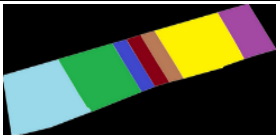 | 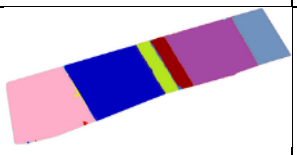 | 82.71 |
| **5** | | 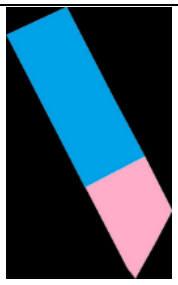 | 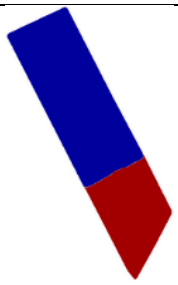 | 99.69 |

| | | | | |
|---|---|---|---|---|
| **6** | | 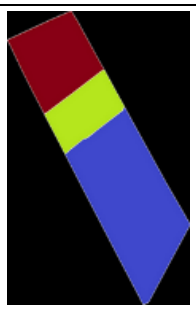 | | 66.04 |
| **7** | 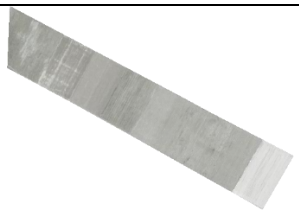 | 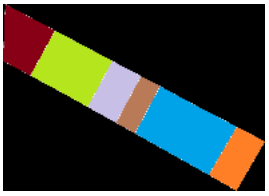 | 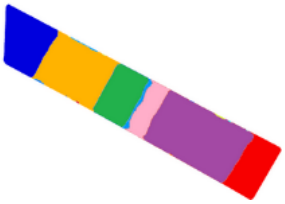 | 96.42 |
| **8** | | 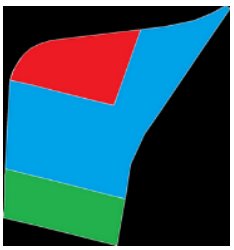 | | 96.10 |
| **9** | | 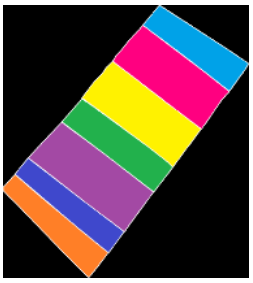 | 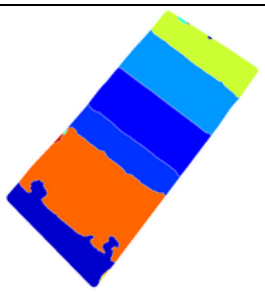 | 80.22 |
| **10** | | | | 96.65 |
| **11** | | 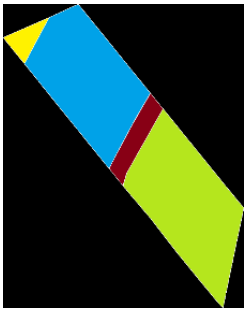 | | 87.31 |

| | | | | |
|---|---|---|---|---|
| **12** | | 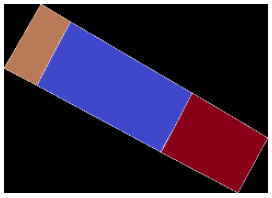 | 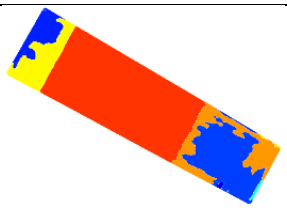 | 83.80 |
| **13** | 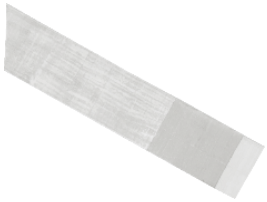 | 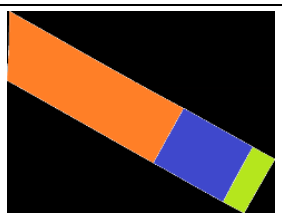 | 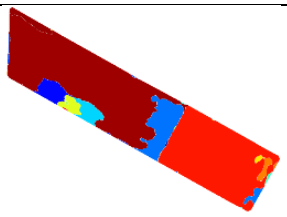 | 35.23 |
| **14** | | 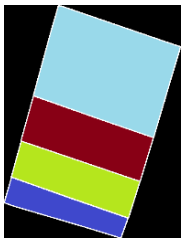 | 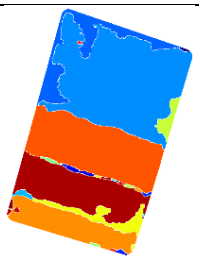 | 91.96 |
| **15** | 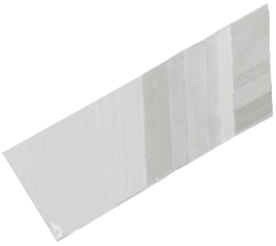 | 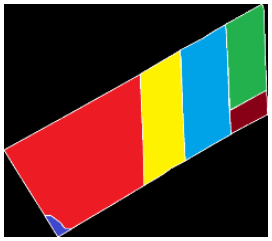 | 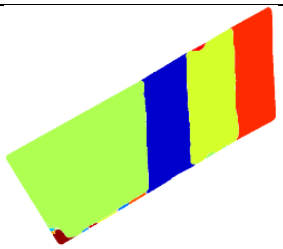 | 77.27 |
| **16** | | 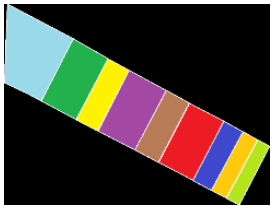 | 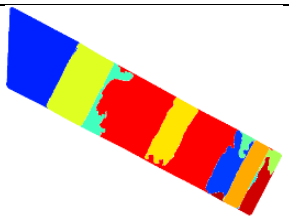 | 61.69 |
| **17** | | 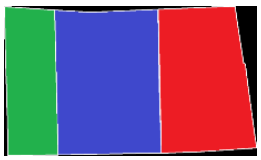 | 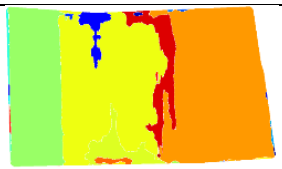 | 92.52 |
| **18** | | 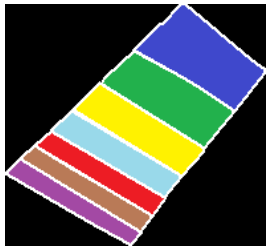 | 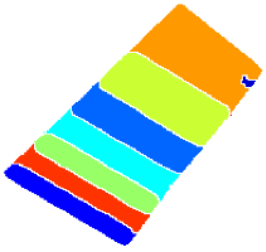 | 95.43 |

| | | | | |
|---|---|---|---|---|
| **19** | 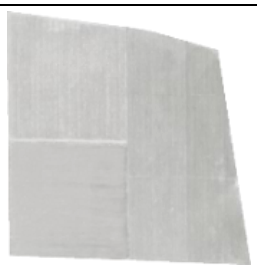 | 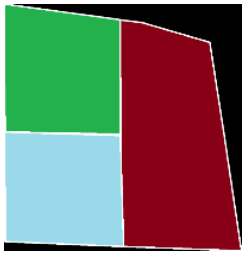 | 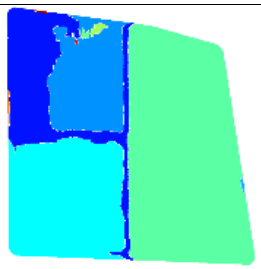 | 64.67 |
| **20** | 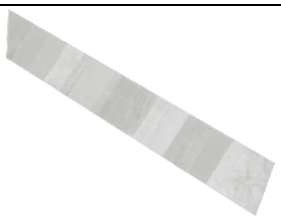 | 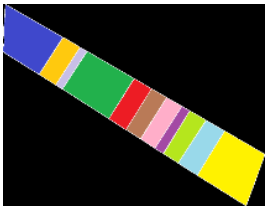 | 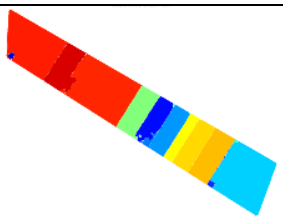 | 87.25 |

**Table 14.** For QuickBird PS imagery the grouping of test fields based on their accuracy values.

| Accuracy | Fields | Total | Percentage |
|---|---|---|---|
| 85 – 100 | #5,#7,#8,#10,#11,#14,#17,#18,#20 | 9 | 45% |
| 70 – 84 | #4,#9,#12,#15 | 4 | 20% |
| 50 – 69 | #2,#3,#6,#16,#19 | 5 | 25% |
| 0 – 49 | #1,#13 | 2 | 10% |
| Total | | 20 | 100% |

### 4.3.4. The Results of Spot5 Multispectral (XS) Images

The results of the Spot5 XS imagery and the reference data are given in Table 15. The grouping of the test fields based on their accuracy values are provided in Table 16. According to Table 16, just 35% of the results have ideal accuracy values (above 85%). But a more exact investigation of the table will approve that all of the 7 fields in this field have accuracies above 90% and another fact that would be approved is that 55% of the fields have accuracies above 80%.

These facts support the reliability of the proposed method in the case of Spot5 XS imagery. By investigating Table 15, it can be seen that there are two fields with more than one over or under segmentation.

In this category (Spot5 XS), the spatial resolution (10m) is rather coarse and therefore each subfield has much fewer pixels in comparison to the other three images which were mentioned earlier. This incident leads to the falling of the accuracy of this data set.

Because each subfield has fewer number of pixels, the lack of 3 or 4 pixels in one subfield can lead to fall down of the accuracy value. For example, consider one of the subfields has only 10 pixels and the operation could find 7 pixels of that subfield. This field wouldn't be considered as true segment in the accuracy assessment operation because it cannot provide the 75% [16] threshold value used in the assessment method.

Also the low resolution of Spot5 images lead to another problem which is the low between-field variation. The original concept of the proposed method is based on the Otsu thresholding method, and as it is mentioned in the section 3.2.1.2, it depends on the brightness value of the pixels. The low between-field variation will lead to low accuracy at the thresholding step, and it affects directly the number of foreground markers and also the result of the watershed segmentation. As it is mentioned at the start of this section and Table 8, Spot5 images have just 1 over-segmented result but 8 under segmented results. This is another proof of the discussed issue.

**Table 15.** The results of Spot5 XS images

| # | Original Field | Reference Segments | Segmentation Result | Accuracy (%) |
|---|---|---|---|---|
| **1** | 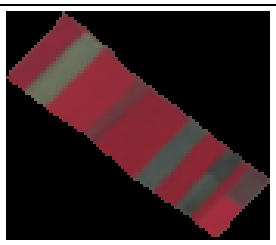 | 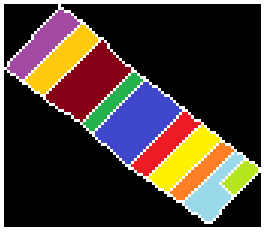 | 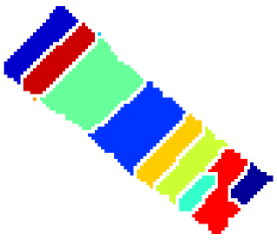 | 72.45 |
| **2** | 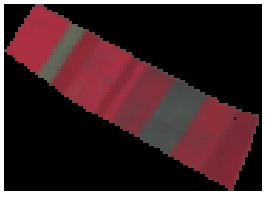 | | | 70.29 |

| | | | | |
|---|---|---|---|---|
| **3** | 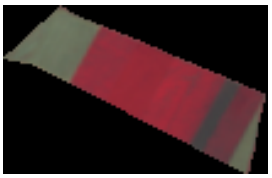 | | 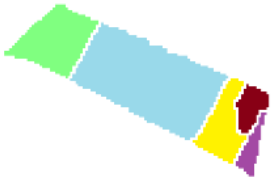 | 57.28 |
| **4** | 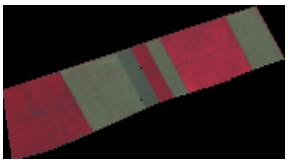 | 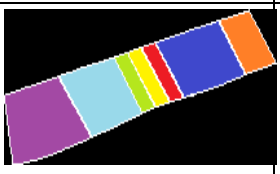 | 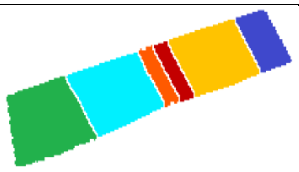 | 82.95 |
| **5** | | | 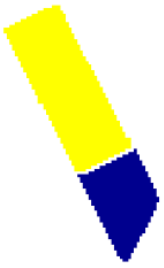 | 98.50 |
| **6** | 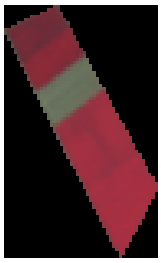 | 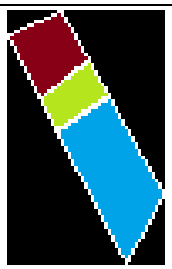 | | 96.83 |
| **7** | | | 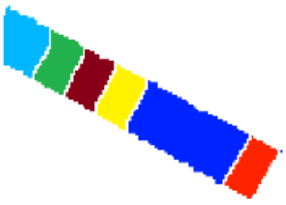 | 95.42 |
| **8** | 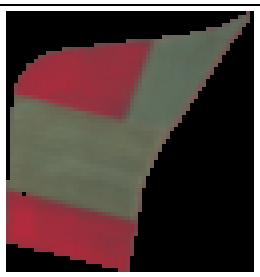 | 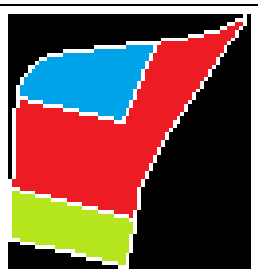 | | 97.14 |
| **9** | 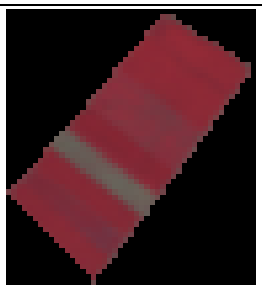 | 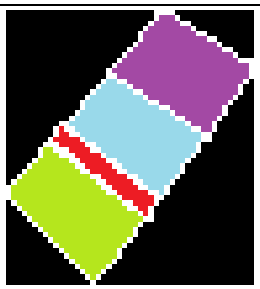 | 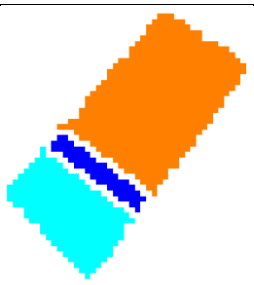 | 59.91 |

| | | | | |
|---|---|---|---|---|
| **10** | | | | 84.37 |
| **11** | | | 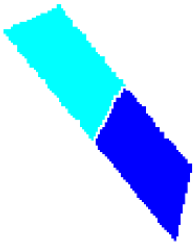 | 95.88 |
| **12** | 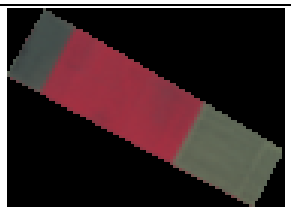 | 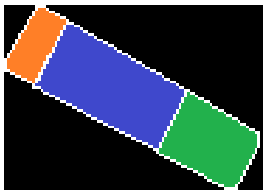 | 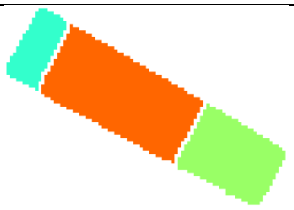 | 95.24 |
| **13** | | | 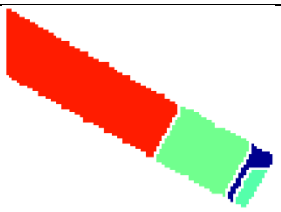 | 83.00 |
| **14** | | 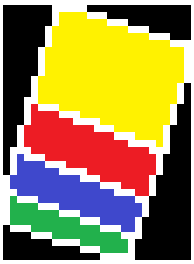 | | 73.22 |
| **15** | 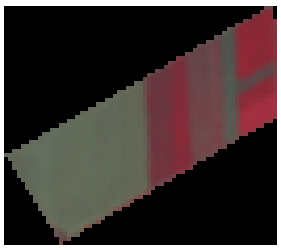 | 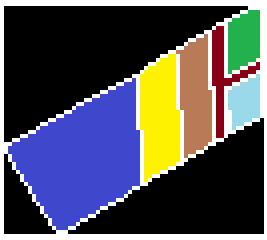 | 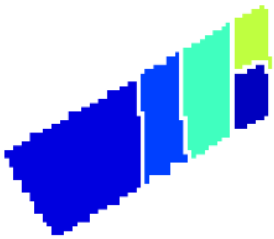 | 74.67 |

| | | | | |
|---|---|---|---|---|
| **16** | 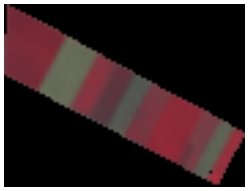 | | 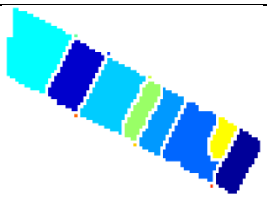 | 77.17 |
| **17** | | 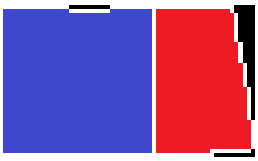 | | 80.65 |
| **18** | 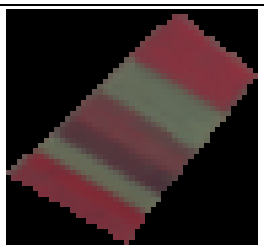 | 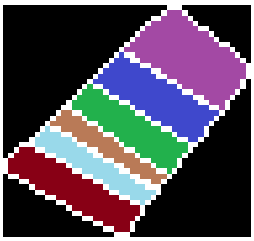 | | 56.11 |
| **19** | | 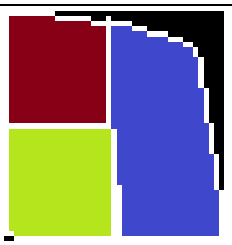 | 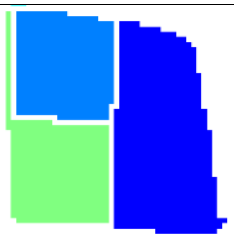 | 91.87 |
| **20** | | 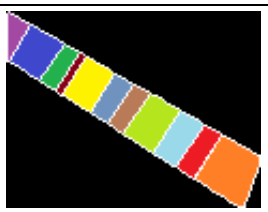 | 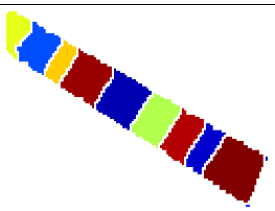 | 77.36 |

**Table 16.** For Spot5 XS image the grouping of the test fields based on their accuracy values

| Accuracy | Fields | Total | Percentage |
|---|---|---|---|
| 85 – 100 | #5,#6,#7,#8,#11,#12,#19 | 7 | 35% |
| 70 – 84 | #1,#2,#4,#10,#13,#14,#15,#16,#17, #20 | 10 | 50% |
| 50 – 69 | #3,#9,#18 | 3 | 15% |
| 0 – 49 | | 0 | 0% |
| Total | | 20 | 100% |

### 4.3.5. Comparison of All Four Images

In this section, a brief investigation of the accuracy of all 20 test fields will be carried out using Table 17. This table compares the grouping results of all four images used.

This table approves that the best result of the proposed method belongs to Ikonos XS data set with 90% of the results having an accuracy above 70%. Spot5 XS, has the second ranking with 85% of the results having an accuracy above 70%. These two categories also do not have any results with an accuracy below 50%.

QuickBird XS and QuickBird PS images have the 3rd and the 4th rankings respectively in this method, with 80% and 65% of the results with an accuracy above 70%.

QuickBird Ps have 7 fields with an accuracy below 70, while this number is 4, 3 and 2 for QuickBird XS, Spot5 XS and Ikonos XS images respectively.

All of these facts support the reliability of the proposed method of this thesis.

**Table 17.** The comparison of the grouping of the test fields based on their accuracies

| Accuracy Range | Spot5 XS | | Ikonos XS | | QuickBird XS | | QuickBird PS | |
|---|---|---|---|---|---|---|---|---|
| | Number of Fields | Percentage | Number of Fields | Percentage | Number of Fields | Percentage | Number of Fields | Percentage |
| 85-100 | 7 | 35 | 15 | 75 | 12 | 60 | 9 | 45 |
| 70-84 | 10 | 50 | 3 | 15 | 4 | 20 | 4 | 20 |
| 50-69 | 3 | 15 | 2 | 10 | 2 | 10 | 5 | 25 |
| 0-49 | 0 | 0 | 0 | 0 | 2 | 10 | 2 | 10 |
| Total | 20 | 100 | 20 | 100 | 20 | 100 | 20 | 100 |

# 5. CONCLUSIONS AND RECOMMENDATIONS

## 5.1. Conclusions

This study proposes an automatic field-based segmentation approach in agricultural fields that stay within the boundaries defined by the roads, ditches, channels, etc. from high resolution satellite images. The segmentation methodology is based on employing Otsu's thresholding method and the image gradient magnitude for implementing the marker controlled watershed segmentation. During segmentation, the result of Otsu's thresholding is used to determine the foreground markers for an improved marker controlled watershed algorithm. The approach starts with transforming an RGB image to an Intensity image and thresholding the image using an iterative two-step Otsu's thresholding method. The foreground markers are then generated to be used in the improved marker controlled watershed algorithm. The watershed algorithm is carried out on the gradient magnitude image by using the foreground markers that are obtained by using an iterative two-step Otsu's algorithm. An accuracy assessment based on polygon matching technique is used to evaluate the results.

The proposed sub-field segmentation approach was tested on a study area using the Spot5 XS image (with 10 meter spatial resolution), the Ikonos XS image (with 4 meter spatial resolution), the QuickBird XS image (with 2.44 meter spatial resolution), and the QuickBird PS image (with 0.61 meter spatial resolution).

The opportunity of having four different spatial resolution images was an advantage that helped better evaluate the developed field-based sub-field extraction approach. The achieved results illustrated that the proposed approach can be reliably performed for the extraction of sub-fields in agricultural areas. Moreover, the method provides promising results even though the results of gradient magnitude is poor. However, if both the gradient magnitude and the Otsu's thresholding method miss to detect a sub-field, then the proposed method may fail to extract that sub-field due to inaccurate generation of the foreground markers which are computed by the iterative Otsu's thresholding method. Yet, based on the results acquired in this study, it is witnessed that the developed approach is highly robust and provides very high accuracies for the extraction of sub-fields from high and very high resolution satellite images. The proposed approach, in which the marker controlled watershed algorithm uses the thresholded image as the foreground markers, can also be

employed for the extraction of manmade objects, such as buildings and roads through object-based segmentation. The results achieved in this study also demonstrate that the marker controlled watershed algorithm has a good potential in image segmentation when the foreground markers are calculated accurately to conduct the growing procedure. Nonetheless, the marker controlled watershed algorithm largely depends on the seeded markers. In this study, this problem has been dealt with by using the output of the iterative Otsu's thresholding method. It was found that using only the Intensity image as the input for gradient magnitude calculation and thresholding may lead to inaccurate results in some cases. The results illustrate that the Sobel operator the performance of which is known to be premier in general to other operators, appears to provide a good performance for calculating the gradient image in agricultural fields. Nonetheless, as shown in this study, the results may also very well appertain on the input image. In this study, the developed automatic iterative Otsu's thresholding algorithm illustrated a good performance for finding the correct number of markers within the permanent boundaries of roads, ditches, channels, etc. Therefore, it can be concluded that the proposed automatic iterative Otsu's thresholding approach was a good choice for the clustering of fields that contain adjacent sub-fields which have greater surface areas, and it does not depend on the number of sub-fields contained within the permanent boundaries. Moreover, it is obvious that the proposed approach has good results on the fields that have large number of sub-fields.

### 5.2. Recommendations

Based on the obtained results and the observations made in this study, the proposed scheme proved to have met its design expectations. However, the followings are recommended for future studies:

1- In this research, the developed method was carried out on the images of agricultural areas that contain fields with a maximum of thirteen sub-fields. It is recommended that the performance of the approach should be examined on areas that contain fields with higher number of sub-fields.

2- In this study, marker controlled watershed algorithm was improved in terms of generating a novel foreground markers and a novel seeding procedure. However, along with the foreground markers, the marker controlled

watershed algorithm also uses the background markers in order to develop the dams for the prevention of extra growing procedure. As a future work, new modifications can be applied on the background markers of the improved marker controlled watershed algorithm to further increase the reliability of the results.

3- In this study, the intensity image is used as the input data for the Otsu's thresholding method and calculating the gradient magnitude. For further investigations, other types of images like an NDVI image or an LAB color space image, or the combination of them, can be used for improving the marker controlled watershed algorithm.
4- In this study, Sobel operator is used for computing the gradient magnitude image. For future studies, other methods can be used for calculating the gradient magnitude image, to see the effect of different operators on the final results.
5- In this research, an iterative Otsu's thresholding method is used for finding the foreground markers. To further improve the efficiency of the proposed approach other alternative methods can be used for finding the foreground markers to increase the accuracy of the final outputs.
6- In this study, a novel improved marker controlled watershed algorithm is used to extract sub-fields within agricultural fields. The proposed method can also be used for the extraction of other manmade or natural objects, such as buildings and roads. Therefore, it is recommended that the developed improved marker controlled watershed algorithm should be carried out for the extraction of different objects to analyze its adaptability in different applications.

# REFERENCES


[1] P. Aplin and P. M. Atkinson, “Predicting missing field boundaries to increase perfield classification accuracy,” *Photogramm. Eng. Remote Sensing*, vol. 70, pp. 141–149, **2004**.

[2] A. J. W. De Wit and J. G. P. W. Clevers, “Efficiency and Accuracy of Per-Field Classification for Operational Crop Mapping,” *Int. J. Remote Sens.*, vol. 25, no. 20, pp. 4091–4112, **2004**.

[3] M. Turker and E. Derenyi, “GIS assisted change detection using remote sensing,” *Geocarto Int.*, vol. 15, pp. 49–54, **2000**.

[4] S. Lang and T. Blaschke, “Bridging remote sensing and GIS - what are the main supportive pillars?,” in *1st International Conference on Object-based Image Analysis (OBIA 2006)*, no. 36, pp. 4–C42. , **2006.**

[5] G. J. Hay and G. Castilla, “Object-based image analysis: strengths, weaknesses, opportunities and threats (SWOT),” in *International Archives of Photogrammetry Remote Sensing and Spatial Information Sciences*, vol. 36, p. 4 , **2006**.

[6] A. Rydberg, G. Borgefors, and S. Member, “Integrated Method for Boundary Delineation of Agricultural Fields in Multispectral Satellite Images,” vol. 39, no. 11, pp. 2514–2520, **2001**.

[7] M. Mueller, K. Segl, and H. Kaufmann, “Edge- and region-based segmentation technique for the extraction of large, man-made objects in high-resolution satellite imagery,” *Pattern Recognit.*, vol. 37, no. 8, pp. 1619–1628, **2004**.

[8] Y. Cheng, “Mean shift, mode seeking, and clustering,” *IEEE Trans. Pattern Anal. Mach. Intell.*, vol. 17, no. 8, pp. 790–799, **1995**.

[9] K. S. FU and J. K. Mui, “A survey of image segmentation,” *Pattern Recognit.*, vol. 13, no. 1, pp. 3–16, **1981**.

[10] N. R. Pal and S. K. Pal, “A review on image segmentation techniques,” *Pattern Recognit.*, vol. 26, no. 9, pp. 1277–1294, **1993**.

[11] E. Petersen, M. D. de Ridder, and H. Handels, “Image Processing with Neural Networks-a Review,” *Pattern Recognit.*, vol. 35, pp. 2279–2301, **2001**.

[12] H. Zhang, J. E. Fritts, and S. A. Goldman, “Image segmentation evaluation: A survey of unsupervised methods,” *Comput. Vis. Image Underst.*, vol. 110, no. 2, pp. 260–280, **2008**.

[13] a. Rosenfeld and M. Thurston, “Edge and Curve Detection for Visual Scene Analysis,” *IEEE Trans. Comput.*, vol. C–20, no. 5, pp. 562–569, **1971**.

[14] S. Shimojo and K. Nakayama, “Experiencing and perceiving visual surfaces,” *Science (80-. ).*, vol. 257, pp. 1357–1363, **1992**.

[15] M. Turker and E. H. Kok, “Automatic Extraction of Sub-Boundaries Within Agricultural Fields From Remote Sensing Images,” in *Center for remote sensing of land surface*, pp. 55–63, **2006**.

[16] M. Turker and E. H. Kok, “Field-based sub-boundary extraction from remote sensing imagery using perceptual grouping,” *ISPRS J. Photogramm. Remote Sens.*, vol. 79, pp. 106–121, **2013**.

[17] M. Zafeiri, “Biomedical Image Segmentation using the Watershed Transform to initialize Region Growing,” Technical University of Crete, **2008**.

[18] Z. Chi, H. Yan, and T. Pham, *Fuzzy Algorithms: With applications to images processing and pattern recognition*. **1996**.

[19] J. Kittler and J. Illingworth, “Minimum error thresholding,” *Pattern Recognit.*, vol. 19, no. 1, pp. 41–47, **1986**.

[20] R. B. Ohlander, “Analysis of natural scenes,” Carnegie Mellon University, **1975**.

[21] M. Cheriet, J. N. Said, and C. Y. Suen, “A recursive thresholding technique for image segmentation,” *IEEE Trans. Image Process.*, vol. 7, no. 6, pp. 918–921, **1998**.

[22] N. Otsu, “A Threshold Selection Method from Gray-Level Histograms,” *IEEE Trans. Syst. Man. Cybern.*, vol. 9, no. 1, pp. 62–66, **1979**.

[23] “http://scipy-lectures.github.io/packages/scikit-image/.” [Online]. Available: http://scipy-lectures.github.io/packages/scikit-image/.

[24] J. M. Prager, “Extracting and labeling boundary segments in natural scenes,” *IEEE Trans. Pattern Anal. Mach. Intell.*, vol. 2, no. 1, pp. 16–27, **1980**.

[25] W. A. Perkins, “Area segmentation of images using edge points,” *IEEE Trans. Pattern Anal. Mach. Intell.*, vol. 2, no. 1, pp. 8–15, **1980**.

[26] “Illustrated Dictionary of Computer Vision.” [Online]. Available: http://homepages.inf.ed.ac.uk/rbf/CVDICT/cve.htm.

[27] K. Cho and P. Meer, “Image Segmentation from Consensus Information,” *Comput. Vis. Image Underst.*, vol. 68, no. 1, pp. 72–89, **1997**.

[28] U. M. Fayyad, G. Piatetsky-Shapiro, P. Smyth, and R. Uthurusamy, *Advances in Knowledge Discovery and Data Mining*. AAAI Press, **1996**.

[29] a. K. Jain, M. N. Murty, and P. J. Flynn, “Data clustering: a review,” *ACM Comput. Surv.*, vol. 31, no. 3, pp. 264–323, **1999**.

[30] J. H. Raymond T Ng, “Efficient and effective clustering methods for spatial data mining,” in *Proceedings of the International Conference on Very Large Data Bases*, pp. 144–155, **1994**.

[31] A. K. Jain and R. C. Dubes, *Algorithms for clustering data*, vol. 1. **1988**.

[32] X. Li, J. Yang, Q. Wang, J. Fan, and P. Liu, “Research and Application of Improved K-means Algorithm Based on Fuzzy Feature Selection,” in *Fuzzy Systems and Knowledge Discovery, 2008. FSKD ’08. Fifth International Conference on*, pp. 401–405, **2008**.

[33] S. S. Khan and A. Ahmad, “Cluster center initialization algorithm for K-means clustering,” *Pattern Recognit. Lett.*, vol. 25, no. 11, pp. 1293–1302, **2004**.

[34] P. S. Bradley and U. M.Fayyad, “Refining Initial Points for K-Means Clustering,” in *15th International Conf. on Machine Learning (ICML98)*, pp. 91–99, **1998**.

[35] K. . Ravichandran and B. Ananthi, “Color skin segmentation using K-means cluster,” *Int. J. Comput. Appl. Math.*, vol. 4, no. 2, pp. 153–157, **2009**.

[36] M. G. C. a Cimino, B. Lazzerini, and F. Marcelloni, “A novel approach to fuzzy clustering based on a dissimilarity relation extracted from data using a TS system,” *Pattern Recognit.*, vol. 39, no. 11, pp. 2077–2091, **2006**.

[37] D. . Hemanth, D. Selvathi, and J. Anitha, “Effective Fuzzy Clustering Algorithm for Abnormal MR Brain Image Segmentation,” in *Advance Computing Conference, 2009. IACC 2009. IEEE International*, pp. 609–614, **2009**.

[38] P. Vasuda, “Improved Fuzzy C-Means Algorithm for MR BrainImage Segmentation,” *Int. J. Comput. Sci. Eng.*, vol. 2, no. 5, pp. 1713–1715, 2010**.**

[39] F. Yarman-Vural and E. Ataman, “Noise, histogram and cluster validity for Gaussianmixtured data,” *Pattern Recognit.*, vol. 20, no. 4, pp. 385–401, **1987**.

[40] “http://www.iro.umontreal.ca/~mignotte/Demo.html.” [Online]. Available: http://www.iro.umontreal.ca/~mignotte/Demo.html.

[41] J. F. Haddon and J. F. Boyce, “Image segmentation by unifying region and boundary information,” *IEEE Trans. Pattern Anal. Mach. Intell.*, vol. 12, no. 10, pp. 929–948, **1990**.

[42] N. W. Campbell, B. T. Thomas, and T. Troscianko, “Automatic segmentation and classification of outdoor images using neural networks,” *Int. J. Neural Syst.*, vol. 8, no. 1, pp. 137–144, **1997**.

[43] N. Papamarkos, C. Strouthopoulos, and I. Andreadis, “Multithresholding of colour and gray-level images through a neural network technique,” *Image Vis. Comput.*, vol. 18, pp. 213–222, **2000**.

[44] J. Roerdink and a Meijster, “The Watershed Transform: Definitions, Algorithms and Parallelization Strategies,” *Fundam. Informaticae*, vol. 41, no. 1–2, pp. 187–228, **2000**.

[45] H. Digabel and C. Lantuejoul, *ITERATIVE ALGORITHMS*, 1st ed. FONTAINEBLEAU, **1977**.

[46] S. Beucher and C. Lantuejoul, “Use of Watersheds in Contour Detection,” *International Workshop on Image Processing: Real-time Edge and Motion Detection/Estimation*. pp. 12–21, **1979**.

[47] J. Serra, *Image Analysis and Mathematical Morphology*, 1st ed. Academic Press, **1984**.

[48] D. Wang, “A multiscale gradient algorithm for image segmentation using watersheds,” *Pattern Recognit.*, vol. 30, pp. 2043–2052, **1997**.

[49] S. Beucher, M. Bilodeau, and X. Yu, “Road segmentation by watershed algorithms,” *Proc. Prometh. Work. Sophia-Antipolis, Fr.*, pp. 1–24, **1990**.

[50] S. Beucher and M. Bilodeau, “Road segmentation and obstacle detection by a fast watershed transformation,” *Proc. Intell. Veh. ’94 Symp.*, **1994**.

[51] Y. Li, L. Zhu, H. Shimamura, and K. Tachibana, “an Integrated System on Large Scale Building Extraction From Dsm,” *Image (Rochester, N.Y.)*, vol. XXXVIII, pp. 35–39, **2010**.

[52] Y. Li, L. Zhu, and H. Shimamura, “Integrated Method of Building Extraction From Digital Surface,” pp. 2–7.

[53] R. M. Lark and H. C. Wheeler, “Precision agriculture,” in *Response*, vol. 1104, pp. 1093–1104, **2003**.

[54] V. Grau, a. U. J. Mewes, M. Alcañiz, R. Kikinis, and S. K. Warfield, “Improved watershed transform for medical image segmentation using prior information,” *IEEE Trans. Med. Imaging*, vol. 23, no. 4, pp. 447–458, **2004**.

[55] H. P. Ng, S. Huang, S. H. Ong, K. C. Foong, P. S. Goh, and W. L. Nowinski, “Medical image segmentation using watershed segmentation with texture-based region merging.,” *Conf. Proc. IEEE Eng. Med. Biol. Soc.*, vol. 2008, pp. 4039–4042, **2008**.

[56] W.-F. Kuo, C.-Y. Lin, and W.-Y. Hsu, “Medical image segmentation using the combination of watershed and fcm clustering algorithms,” *Int. J. Innov. Comput. Inf. Control.*, vol. 7, no. 9, pp. 5255–5267, **2011**.

[57] A. Watson, “A new method of classification for Landsat data using the ‘watershed’ algorithm,” *Pattern Recognit. Lett.*, vol. 6, pp. 15–19, **1987**.

[58] G. Castilla, J. Geoffrey, and J. R. Ruiz-gallardo, “Size-constrained Region Merging ( SCRM ): An Automated Delineation Tool for Assisted Photointerpretation,” *Photogramm. Eng. Remote Sens.*, vol. 74, no. 4, pp. 409–419, **2008**.

[59] A. Plaza, P. Martínez, R. Pérez, and J. Plaza, “Spatial/spectral endmember extraction by multidimensional morphological operations,” *IEEE Trans. Geosci. Remote Sens.*, vol. 40, no. 9, pp. 2025–2041, **2002**.

[60] P. Soille, “Morphological partitioning of multispectral images,” *J. Electron. Imaging*, vol. 5, pp. 252–265, **1996**.

[61] A. WATSON, R. VAUGHAN, and M. POWELL, “Classification using the watershed method,” *Int. J. Remote Sens.*, vol. 13, pp. 1881–1890, **1992**.

[62] J.-F. Rivest, S. Beucher, and J. Delhomme, “Marker-controlled segmentation: an application to electrical borehole imaging,” *J. Electron. Imaging*, vol. 1, no. 2, pp. 136–142, **1992**.

[63] S. Lefèvre, “Knowledge from Markers in Watershed Segmentation,” *Knowl. Creat. Diffus. Util.*, pp. 1–8, **2007**.

[64] A. Kaur and A. Verma, “The Marker-Based Watershed Segmentation- A Review,” vol. 3, no. 3, pp. 171–174, **2013**.

[65] R. Srisha and A. M. Khan, “Morphological Operations for Image Processing : Understanding and its Applications Morphological Operations for Image Processing : Understanding and its Applications,” in *NCVSComs-13*, pp. 17–19, **2013**.

[66] L. Vincent and P. Soille, “Watersheds in digital spaces: An efficient algorithm based on immersion simulations,” *IEEE Transactions on Pattern Analysis and Machine Intelligence*, vol. 13, no. 6. pp. 583–598, **1991**.

[67] K. Parvati, B. S. Prakasa Rao, and M. Mariya Das, “Image segmentation using gray-scale morphology and marker-controlled watershed transformation,” *Discret. Dyn. Nat. Soc.*, vol. 2008, **2008**.

[68] T. Carron and P. Lambert, “Color edge detector using jointly hue, saturation and intensity,” *Proc. 1st Int. Conf. Image Process.*, vol. 3, pp. 977–981, **1994**.

[69] R. C. Gonzalez, R. E. Woods, and B. R. Masters, *Digital image processing, third edition.*, vol. 14, no. 2. **2008**.

[70] W. **K**. Pratt, *Digital image processing : PIKS scientific inside*, 4th ed. Wiley, 2007.

[71] J. R. Parker, *Algorithms for Image Processing and Computer Vision*, 2nd ed. Wiley, **2011**.

[72] C. Solomon and T. Breckon, *Fundamentals of Digital Image Processing*, 1st ed. Wiley-Blackwell, **2010**.

[73] P. Soille, *Morphological Image Analysis*, 1st ed. Springer, **1999**.

[74] H. Zhou, J. Wu, and J. Zhang, *Digital Image Processing-Part Two*. **2010**.

[75] F. Y.Shih, *Image Processing and Mathematical Morphology fundamentals and applications*, 1st ed. CRC press, **2009**.

[76] N. R.Chrisman, “Modelling error overlaid categorical maps,” *Accuracy Spat. database*, no. London, pp. 21–34, **1989**.

[77] L. L. F. Janssen and M. Molenaar, “Terrain objects, their dynamics and their monitoring by the integration of GIS and remote sensing,” *IEEE Trans. Geosci. Remote Sens.*, vol. 33, no. 3, pp. 749–758, **1995**.

[78] M. Turker and A. Ozdarici, “Field-based crop classification using SPOT4, SPOT5, IKONOS and QuickBird imagery for agricultural areas: a comparison study,” *Int. J. Remote Sens.*, vol. 32, no. 24, pp. 9735–9768, **2011**.

# CURRICULUM VITAE

## Credentials


| | | |
|---|---|---|
| Name, Surname | : | Alireza RAHIMZADEGANASL |
| Place of Birth | : | Tehran, Iran |
| Marital Status | : | Single |
| Email | : | a.lvl.rahimzadegan@gmail.com |
| Address | : | Geomatics Engineering Department of Hacettepe University Beytepe – ANKARA |


## Education

| | | |
|---|---|---|
| High School | : | Chamran High School, Iran |
| BSc. | : | Surveying Engineering, Islamic Azad University, Iran |
| MSc. | : | – |
| PhD. | : | – |

## Foreign Languages

English, Persian, Turkish

## Work Experiences

–

## Area of Experiences

–

## Project and Budgets

–

## Publications

–

## Oral and Poster Presentations

–